

STRONGLY INTERACTING VECTOR BOSONS AT TeV $e^\pm e^-$ LINEAR COLLIDERS

E. BOOS^{1,2}, H.-J. HE³, W. KILIAN⁴, A. PUKHOV², C.-P. YUAN⁵,
AND P.M. ZERWAS³

¹Technische Hochschule Darmstadt, Schloßgartenstr. 9
D-64289 Darmstadt, Germany

²Institute of Nuclear Physics, Moscow State University
119899 Moscow, Russia

³Deutsches Elektronen-Synchrotron DESY
D-22603 Hamburg, Germany

⁴Institut für Theoretische Physik, Universität Heidelberg, Philosophenweg 16
D-69120 Heidelberg, Germany

⁵Department of Physics and Astronomy, Michigan State University
East Lansing, Michigan 48824, USA

ABSTRACT

In the absence of light Higgs bosons, the W and Z bosons become strongly interacting particles at energies of about 1 TeV. If the longitudinal W, Z components are generated by Goldstone modes associated with spontaneous symmetry breaking in a new strong interaction theory, the quasi-elastic W, Z scattering amplitudes can be predicted as a systematic chiral expansion in the energy. We study the potential of TeV e^+e^- and e^-e^- linear colliders in investigating these scattering processes. We estimate the accuracy with which the coefficients of the chiral expansion can be measured in a multi-parameter analysis. The measurements will provide us with a quantitative test of the dynamics underlying the W, Z interactions.

1. Introduction

Elastic scattering amplitudes of massive vector bosons grow indefinitely with energy if they are calculated as a perturbative expansion in the coupling of a non-abelian gauge theory. As a result, they manifestly violate unitarity beyond a critical energy scale $\sqrt{s_c}$ [1]. In fact, the S -wave scattering amplitude of longitudinally polarized W, Z bosons in the isoscalar channel $(2W^+W^- + ZZ)/\sqrt{3}$,

$$a_0^0(s) = \frac{\sqrt{2}G_F s}{8\pi} + \mathcal{O}(g^2, g'^2) \quad (1)$$

must be bounded by unity. Unitarity therefore is violated for energies in excess of

$$\sqrt{s_c} \sim 1.2 \text{ TeV} \quad (2)$$

in WW scattering.

This problem can be solved in two different ways. In the Standard Model [2] a novel scalar particle, the Higgs boson, is introduced to restore unitarity at high energies [3,4]. The additional contribution due to the exchange of this particle in the scattering amplitude of longitudinal vector bosons cancels the asymptotic rise of the Yang-Mills amplitude if the coupling of the Higgs particle to the W, Z bosons is chosen properly. In that case, the tree-level amplitude approaches a constant value. Electroweak observables in the fermion/gauge boson sector of the Standard Model are affected by radiative corrections which depend logarithmically on the Higgs boson mass M_H . From the high-precision data at LEP1, SLC, and the Tevatron, an upper limit of $M_H < 550 \text{ GeV}$ has been derived at the 2σ level [5]. This limit is not sharp: Excluding one or two observables from the analysis weakens the bound significantly [6]. In a cautious conclusion the experimental limit may therefore be interpreted within the minimal model as indicative for a scale $< \mathcal{O}(1 \text{ TeV})$.

However, there exists a second solution to the unitarity problem. If the Higgs boson is not realized in Nature, the W bosons become strongly interacting particles at TeV energies. In such a scenario the experimental upper bound of $\sim 1 \text{ TeV}$ can be re-interpreted as the cut-off scale up to which the Standard Model of fermions and vector bosons may be extended before new physical phenomena become apparent. Such novel strong interactions of the W bosons may be indicated by slight deviations of the static electroweak W, Z parameters from the predictions in the Standard Model, *i.e.*, for the oblique parameters, the Z charge, the magnetic dipole, and

the electric quadrupole moments of the W^\pm bosons [7,8,9]. However, besides the production of triple gauge bosons in e^+e^- annihilation [10], the classical test ground for these interactions is the elastic and quasi-elastic $2 \rightarrow 2$ scattering experiments of the W^\pm and Z bosons

$$WW \rightarrow WW \tag{3}$$

where W generically denotes the particles W^\pm, Z .

It is natural, though not compulsory, to trace back the strong interactions of the W bosons to a new fundamental strong interaction characterized by a scale of order 1 TeV [11]. If the Lagrangean of the underlying theory is globally chiral-invariant, this symmetry may be broken spontaneously. The Goldstone bosons associated with the spontaneous symmetry breaking can be absorbed by the gauge bosons to generate the masses and to build up their longitudinal degrees of freedom. It may be assumed in this scenario that the breaking pattern of the chiral symmetry in the strongly interacting sector is such that $SU(2) \times SU(2) \rightarrow SU(2)_c$ leaves the isospin group $SU(2)_c$ unbroken. This custodial $SU(2)_c$ symmetry [11] automatically ensures that the ρ parameter, the ratio of the NC to CC couplings, is unity up to small perturbative corrections. This condition [12] is strongly supported by the electroweak precision data. The fact that in such a scenario the longitudinally polarized W bosons are associated with the Goldstone modes of chiral symmetry breaking, has far-reaching consequences which are formalized in the Equivalence Theorem [4,13,14]. This mechanism can be exploited to predict the scattering amplitudes of the W_L bosons for high energies below the mass scale of new resonances¹. Expanding the scattering amplitudes in powers of the energy \sqrt{s} , the leading term is parameter-free, thus being a consequence *per se* of the chiral symmetry breaking mechanism, independent of the particular dynamical theory. The higher-order terms in the chiral expansion depend on new coefficients which reflect the detailed structure of the underlying strong-interaction theory. With rising energy they may evolve towards a resonant behavior, in the scalar or vector channels for instance.

To study potentially strong interactions between W bosons requires energies in the TeV range. They will be provided by the pp collider LHC and by future e^+e^- linear colliders which will operate in the second phase at energies of 1.5 to 2 TeV, see *e.g.* Ref.[15]. Longitudinal W bosons are radiated off quarks and electrons/positrons with a probability $g^2/16\pi^2 \sim 3 \times 10^{-3}$;

¹This is the analog to low-energy pion physics below the ρ resonance of QCD, in which the pions are the Goldstone bosons associated with the spontaneous chiral $SU(2) \times SU(2)$ symmetry breaking.

since the Z charge of leptons is small, the radiation of Z bosons is suppressed compared to W bosons. The following (quasi-)elastic processes can be studied in e^+e^- and e^-e^- collisions [16, 17,18]:

$$\begin{aligned}
e^+e^- &\rightarrow \bar{\nu}_e\nu_e W^+W^- & : & W^+W^- \rightarrow W^+W^- \\
e^+e^- &\rightarrow \bar{\nu}_e\nu_e ZZ & : & W^+W^- \rightarrow ZZ \\
e^-e^- &\rightarrow \nu_e\nu_e W^-W^- & : & W^-W^- \rightarrow W^-W^-
\end{aligned} \tag{4}$$

It turns out that the rates for these processes are sufficiently large for thorough analyses at e^+e^- c.m. energies of $\sqrt{s} \sim 1$ TeV and above. Other processes involving initial state Z bosons,

$$\begin{aligned}
e^+e^- &\rightarrow \bar{\nu}_e e^- W^+Z & : & W^+Z \rightarrow W^+Z \\
e^+e^- &\rightarrow e^+e^- ZZ & : & ZZ \rightarrow ZZ
\end{aligned} \tag{5}$$

are suppressed for the reasons discussed above. Nevertheless, they must be investigated to achieve a complete determination of the quartic gauge interactions in next-to-leading order of the chiral expansion. Since all basic scattering processes (4) and (5) lead to different final states, they can be disentangled in principle [though this may not be so straightforward in practice since the final state electrons and positrons may be lost in the forward directions].

The main objective of the present analysis are theoretical predictions for the processes (4) and (5) in the region where the W, Z bosons become strongly interacting but the energies do not reach yet the resonance region, which may be delayed until a scale of $4\pi v \sim 3$ TeV is approached. We study the predictions in leading order of the chiral expansion and analyze the sensitivity to next-to-leading order contributions². This will enable us to estimate the accuracy with which the parameter-free leading-order amplitudes can be measured. If the Higgs mechanism is not realized in Nature, these analyses will shed light on the symmetry structure and the basic physical mechanism that provides masses to the fundamental electroweak bosons. Alternative approaches that are not based on chiral symmetry breaking, would in general lead to quite different predictions for WW scattering amplitudes.

2. Chiral Lagrangeans

For theories in which the chiral symmetry is broken spontaneously, *i.e.*, $SU(2) \times SU(2) \rightarrow SU(2)_c$, effective Lagrangeans can be defined for the associated Goldstone fields. They correspond to expansions in the dimensions of the field operators, or equivalently in the energy \sqrt{s}

²Preliminary results of this study have been presented in Ref.[19].

in momentum space [20,21]. This systematic expansion leads to a parameter-free leading-order interaction in the Lagrangean, supplemented by higher-order terms which reflect the detailed structure of the underlying strong interaction theory. Thus the leading-order interaction is a direct model-independent consequence of chiral symmetry breaking *sui generis*. The Equivalence Theorem then allows to re-interpret scattering amplitudes derived for the Goldstone particles as equivalent to the scattering amplitudes of the longitudinally polarized W, Z particles for asymptotic energies $E(W, Z) \gg M_{W,Z}$.

The kinetic terms of the gauge fields and the first terms in the chiral Lagrangean of the Goldstone fields are given by the following expansion:

$$\begin{aligned} \mathcal{L} &= \mathcal{L}_g + \mathcal{L}_e \\ &+ \mathcal{L}_0 + \mathcal{L}_4 + \mathcal{L}_5 + \dots \end{aligned} \quad (6)$$

\mathcal{L}_g denotes the kinetic $W^{\pm,3}$ and B field Lagrangeans³. The $SU(2) \times U(1)$ gauge fields are coupled to the matter fields through covariant derivatives in \mathcal{L}_e . These two parts of the Lagrangean are given by the expressions

$$\mathcal{L}_g = -\frac{1}{8}\text{tr}[W_{\mu\nu}^2] - \frac{1}{4}B_{\mu\nu}^2 \quad (7)$$

$$\mathcal{L}_e = \bar{e}_L i \not{D} e_L + (\text{L} \leftrightarrow \text{R}) \quad (8)$$

with the usual definition of the covariant $SU(2) \times U(1)$ derivative in terms of the vector fields, the $SU(2)$ generators T^a , and the hypercharge Y :

$$iD_\mu = i\partial_\mu + g\vec{T} \cdot \vec{W}_\mu - g'Y B_\mu \quad (9)$$

In the general R_ξ gauge the Goldstone fields are described by the unitary matrix⁴

$$U = \exp[-i\vec{w} \cdot \vec{\tau}/F] \quad (10)$$

The custodial-symmetric dimension-2 operator of the Goldstone fields is then given by

$$\mathcal{L}_0 = \frac{F^2}{4}\text{tr}[D_\mu U^\dagger D^\mu U] \quad (11)$$

³The complete Lagrangean is understood to contain the usual gauge-fixing and ghost terms.

⁴In the Standard Model, U is the Goldstone boson matrix which generates the Higgs isodoublet field from the real Higgs field in the R_ξ gauges.

The coupling between the Goldstone particles and the W , B gauge fields is parameterized by the coefficient F . The value of this parameter is fixed by the measured W or Z masses,

$$\mathcal{L}_0 = M_W^2 W^+ W^- + \frac{1}{2} M_Z^2 Z^2 + \dots \quad (12)$$

so that the experimental value

$$F = (\sqrt{2} G_F)^{-1/2} = 246 \text{ GeV} \quad (13)$$

can be derived for F from the Fermi constant. In the Standard Model, F is replaced by the expectation value v of the Higgs field in the ground state, $F = v$. However, the physical interpretation of these parameters is completely different in the two scenarios⁵.

A vector field V_μ can be defined by the Goldstone fields as

$$V_\mu = U^\dagger D_\mu U \quad (14)$$

corresponding to the derivative $\partial_\mu \vec{w} + \dots$ for small field strengths. From the vector field two independent dimension-4 operators may be formed

$$\mathcal{L}_4 = \alpha_4 \text{tr} [V_\mu V_\nu]^2 \quad (15)$$

$$\mathcal{L}_5 = \alpha_5 \text{tr} [V_\mu V^\mu]^2 \quad (16)$$

which describe the first two non-leading and model-dependent terms in the chiral expansion. The two interaction terms \mathcal{L}_4 and \mathcal{L}_5 are custodial symmetric, leaving the value $\rho = 1$ unchanged. Since they involve at least a quartic coupling of the Goldstone particles, they affect in lowest order only $2 \rightarrow 2$ scattering processes but do not affect the trilinear vertices. Thus, α_4 and α_5 can only be determined in $WW \rightarrow WW$ scattering. [Additional dimension-4 operators affect the trilinear couplings; in this analysis they are assumed to be pre-determined by standard methods such as WW pair production in e^+e^- annihilation.]

We assume that all higher-order coefficients in the chiral expansion are much smaller than unity. Even though a gauge-symmetric chiral Lagrangean can be defined formally for any theory with a particular particle content, this is meaningful only if the chiral series can be truncated at a fixed operator dimension ($d = 4$ for our purpose) and still higher orders can be neglected.

⁵From now on, we will nevertheless adopt the symbol v to characterize the weak-interaction scale, as generally done in the literature.

However, if the concept of spontaneous chiral symmetry breaking were not realized in Nature, higher-order coefficients would be so large that an infinite number of terms would enter even at the W, Z mass scale. In that case, the above effective-theory formalism must be abandoned.

From the magnitude of loop effects which carry a factor $1/16\pi^2$ together with an additional power of s/v^2 , the largest value of \sqrt{s} for a chiral expansion to be valid may be estimated [22] as $\sqrt{s} \lesssim 4\pi v \sim 3$ TeV. Thus, if the coefficients α_i in the chiral expansion were experimentally required to be substantially larger than $1/16\pi^2$, new resonance effects would already appear below the 3 TeV scale, *e.g.*, thresholds for resonance production would become visible in the intermediate range between about 1 and 3 TeV.

Although the 't Hooft-Feynman gauge turns out to be most convenient for the computation method described below (Sec.5.), all observable quantities can be calculated equally well within the unitary gauge in which the Goldstone fields \vec{w} are set to zero. In this gauge the physical content of the various terms becomes more transparent: The standard vector boson interactions are determined by the Yang-Mills kinetic Lagrangean alone, \mathcal{L}_0 just provides the W, Z masses, and the new dimension-4 operators $\mathcal{L}_{4,5}$ are recognized as two independent contact-interaction terms for the W, Z vector bosons:

$$\mathcal{L}_0 = M_W^2 W^+ W^- + \frac{1}{2} M_Z^2 Z^2, \quad (17)$$

$$\mathcal{L}_4 = \alpha_4 \left[\frac{g^4}{2} [(W^+ W^-)^2 + (W^{+2})(W^{-2})] + \frac{g^4}{c_w^2} (W^+ Z)(W^- Z) + \frac{g^4}{4c_w^4} Z^4 \right], \quad (18)$$

$$\mathcal{L}_5 = \alpha_5 \left[g^4 (W^+ W^-)^2 + \frac{g^4}{c_w^2} (W^+ W^-) Z^2 + \frac{g^4}{4c_w^4} Z^4 \right], \quad (19)$$

[$c_w^2 = 1 - \sin^2 \theta_w$ and $g^2 = e^2 / \sin^2 \theta_w$]. The contact terms introduce all possible quartic couplings $W^+ W^- W^+ W^-$, $W^+ W^- Z Z$, and $Z Z Z Z$ among the weak gauge bosons, that are compatible with charge conservation and custodial $SU(2)_c$ symmetry.

3. WW scattering

From the effective chiral Lagrangean, the $2 \rightarrow 2$ (quasi-)elastic WW scattering amplitudes can easily be derived. As shown generically in Fig.1, they involve s -channel, t/u -channel exchange diagrams, and the non-abelian quartic boson coupling, with their sum growing asymptotically proportional to s . The additional quartic contributions introduced by \mathcal{L}_4 and \mathcal{L}_5 rise proportional to s^2 . The maximal power of s is realized only for amplitudes in which all four vector

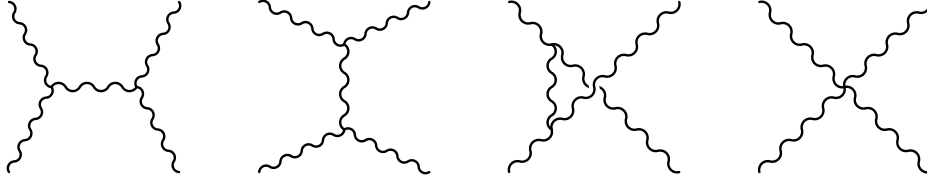


Figure 1: *Feynman graphs for (quasi-)elastic WW scattering.*

bosons are longitudinally polarized; replacing any longitudinally polarized external particle by a transversely polarized particle removes one factor of \sqrt{s}/v ; at the same time an additional power of the weak couplings g, g' is introduced. [In the extreme forward and backward directions where t, u are of the order $M_{W,Z}^2$, the power counting is invalid and both longitudinal and transversal degrees of freedom contribute with comparable magnitude.]

It follows [1,13] from analyticity, crossing symmetry, CP invariance, and custodial symmetry, that to leading order in the Yang-Mills couplings all (quasi-)elastic amplitudes can be expressed in terms of a single function $A(s, t, u)$ which is symmetric with respect to the exchange ($t \leftrightarrow u$). This function is analytic in the Mandelstam variables s, t, u apart from the usual one-particle pole and two-particle cut singularities. The Mandelstam variables are given by the total energy and the momentum transfer in the scattering processes: $s = E_{c.m.}^2$, $t(u) \approx -s(1 \mp \cos \theta)/2$ for $|s|, |t|, |u| \gg M_W^2$. The amplitudes of the scattering processes (4) and (5) can be derived from the master amplitude A in the following way:

$$A(W^+W^- \rightarrow ZZ) = A(s, t, u) \quad (20)$$

$$A(W^+W^- \rightarrow W^+W^-) = A(s, t, u) + A(t, s, u) \quad (21)$$

$$A(W^-W^- \rightarrow W^-W^-) = A(t, s, u) + A(u, s, t) \quad (22)$$

and

$$A(W^+Z \rightarrow W^+Z) = A(t, s, u) \quad (23)$$

$$A(ZZ \rightarrow ZZ) = A(s, t, u) + A(t, s, u) + A(u, s, t) \quad (24)$$

To leading order in the energy expansion the amplitude $A(s, t, u)$ is reduced to the simple expression

$$A(s, t, u)_{\text{LO}} = \frac{s}{v^2} \quad (25)$$

which is parameter-free. The next-to-leading order terms modify this result, and the final tree-level expression is given to order s^2 by

$$A(s, t, u) = \frac{s}{v^2} + \alpha_4 \frac{4(t^2 + u^2)}{v^4} + \alpha_5 \frac{8s^2}{v^4} \quad (26)$$

The relations (20–24) for the amplitudes are preserved by loop corrections and they are valid to all orders for chirally-symmetric strong interactions. There are, however, additional perturbative corrections which are proportional to the Yang-Mills couplings g, g' , with the g' coupling breaking the custodial symmetry. Amplitudes involving transversely polarized vector bosons, which are subleading both for high energies and in the weak coupling expansion, do not respect the relations (20–24).

It is instructive to analyze the angular momentum states that are populated in WW scattering. The helicity analysis [23] of the scattering amplitudes leads to the following decomposition in the angular momentum

$$A(00|00) = \sum_J A_J(00|00) d_{00}^J(\theta) \quad (27)$$

for longitudinally polarized vector bosons, where $d_{00}^J = P_J(\cos \theta)$.

Choosing the process $W^+W^- \rightarrow ZZ$ for example, the gauge contributions to the amplitudes involve t - and u -channel exchange diagrams, giving rise to arbitrarily high orbital angular momentum states. Therefore we decompose the amplitude with respect to spin only, *i.e.*, the residues of the poles for t/u -channel diagrams are expanded:

$$A_J = \frac{s^2}{4M_W^4} \left[g^2 c_w^4 \left(\frac{s}{2(t - M_W^2)} \hat{A}_t + \frac{s}{2(u - M_W^2)} \hat{A}_u + \hat{A}_c \right) + g^4 \left(\alpha_4 \hat{A}_4 + \alpha_5 \hat{A}_5 \right) \right]. \quad (28)$$

The subscripts t, u, c for \hat{A} denote the t, u exchange and the four-boson contact terms, respectively (Tab.1)⁶.

In the spin amplitudes, the contact term contains angular momenta $J = 0$ and 2 . In the t/u channel diagrams the additional vector boson in the intermediate state populates, together with the external vector bosons, the states up to $J = 3$. In the limit $|s|, |t|, |u| \gg M_W^2$ the leading s^2 behavior cancels for $\alpha_4 = \alpha_5 = 0$; however, in the forward/backward regions ($|t|, |u| \sim M_W^2$) this cancellation needs not occur. In other processes such as $W^+W^- \rightarrow W^+W^-$ there is an additional s -channel diagram which is purely spin-1, since a single vector boson Z/γ is exchanged.

⁶For the process $W^+W^- \rightarrow W^+W^-$, the complete decomposition is given in the Appendix.

	\hat{A}_t	\hat{A}_u	\hat{A}_c	\hat{A}_4	\hat{A}_5
$J = 0$	$-\frac{20}{3}$	$-\frac{20}{3}$	$-\frac{16}{3}$	$\frac{8}{3}$	8
1	$\frac{44}{5}$	$-\frac{44}{5}$	0	0	0
2	$-\frac{4}{3}$	$-\frac{4}{3}$	$\frac{4}{3}$	$\frac{4}{3}$	0
3	$-\frac{4}{5}$	$\frac{4}{5}$	0	0	0

Table 1: *Amplitude decomposition for the process $W^+W^- \rightarrow ZZ$ in the limit $E \gg M_W$.*

Given the helicity amplitudes, the differential cross sections can be written as

$$\frac{d\sigma}{d\cos\theta}(W_{\lambda_1}W_{\lambda_2} \rightarrow W_{\lambda_3}W_{\lambda_4}) = \frac{1}{32\pi s} |A(\lambda_1\lambda_2, \lambda_3\lambda_4)|^2. \quad (29)$$

This cross section can easily be integrated over all angles,

$$\sigma(W_{\lambda_1}W_{\lambda_2} \rightarrow W_{\lambda_3}W_{\lambda_4}) = \frac{\eta}{32\pi s} \int_{-1}^1 d(\cos\theta) |A(\lambda_1\lambda_2, \lambda_3\lambda_4)|^2 \quad (30)$$

where $\eta = \frac{1}{2}(1)$ accounts for (non-)identical particles in the final state.

Even though the longitudinal helicities build up the asymptotically leading cross section $\sigma(W_LW_L \rightarrow W_LW_L)$, it cannot be identified with the total cross section without applying angular cuts for non-asymptotic energies since the forward peak for the scattering of transversely polarized W bosons gives rise to additional large contributions to the total cross section.

Interference effects between different helicity amplitudes in the initial state have to be taken into account in the non-asymptotic regime. Since the W bosons are radiated off the electrons and positrons, a coherent mixture of $W_{\lambda_1}W_{\lambda_2}$ helicity states is generated with λ_1 and $\lambda_2 = \pm, 0$. Interference effects in the final $W_{\lambda_3}W_{\lambda_4}$ state need only be included if the angular and energy distributions of the leptons or jets in the W_3, W_4 decays are analyzed explicitly.

4. Equivalent particle approximation

The elastic scattering of W bosons at high energies will be studied in TeV e^+e^- and e^-e^- collisions. At high energies electron/positron beams split for a long time into (neutrino + W) or (electron/positron + Z) pairs. In fact, if the transverse momentum in the splitting process is p_\perp , the lifetime of the split state is of order $\tau \sim E_e/(p_\perp^2 + M_W^2)$ in the laboratory, which is large for high electron/positron energies. With $E_e = 800$ GeV the lifetime $\tau \sim 10^{-1}$ GeV $^{-1}$ is

an order of magnitude longer than the weak interaction scale $\tau_w \sim M_W^{-1} \sim 10^{-2} \text{ GeV}^{-1}$. The W bosons can therefore be approximately treated as equivalent particles [24], similar to the equivalent photon approximation in QED [25]. Moreover, the splitting probability is maximal for small transverse momenta $p_\perp \lesssim M_W$. In the final picture, the W bosons can be treated as real particle beams which accompany the parent e^\pm beams in the accelerator.

The energy spectrum of the W bosons can conveniently be determined, in the spirit of the discussion above, by old-fashioned perturbation theory [26] with the result [24]:

1. *Transversely polarized W^\pm bosons (leading logarithmic approximation):*

$$f_{W/e}^T(x) = \frac{\alpha}{4\pi s_w^2} \frac{1 + (1-x)^2}{2x} \ln \frac{\hat{s}}{M_W^2} \quad (31)$$

For e^- beams, the term ~ 1 corresponds to negative helicity of the W boson, while the term $\sim (1-x)^2$ corresponds to positive helicity, suppressed for $x \rightarrow 1$ by the conservation of angular momentum. [The role of the helicities is interchanged for e^+ beams.] The spectrum increases with the logarithm of the energy, which is a consequence of the unlimited transverse momentum of the point-like coupling in the splitting process.

2. *Longitudinally polarized W^\pm bosons:*

$$f_{W/e}^L(x) = \frac{\alpha}{4\pi s_w^2} \frac{1-x}{x} \quad (32)$$

Since the emission of longitudinally polarized W bosons is suppressed for large transverse momentum, the longitudinal spectra are not logarithmically enhanced.

The fraction of energy transferred from the initial lepton to the W boson is denoted by x , with $0 \leq x \leq 1$.

In the equivalent particle approximation the cross section $d\sigma$ for the colliding beam process, such as

$$e^+e^- \rightarrow \bar{\nu}_e \nu_e W^+ W^- \quad \text{via} \quad W^+ W^- \rightarrow W^+ W^- \quad (33)$$

can be obtained by convoluting the cross section $d\hat{\sigma}$ of the WW subprocess with the spectra of the two initial-state W bosons:

$$d\sigma[e^+e^- \rightarrow \bar{\nu}_e \nu_e W^+ W^-] = \int_0^1 dx_1 \int_0^1 dx_2 f_{W/e}(x_1) f_{W/e}(x_2) d\hat{\sigma}[W^+ W^- \rightarrow W^+ W^-; \hat{s} = x_1 x_2 s] \quad (34)$$

The c.m. invariant energy of the subprocess is given by $\sqrt{\hat{s}} = \sqrt{x_1 x_2 s}$. The fixing of final-state observables Ω can be implemented by restricting the integration over the spectra appropriately:

$$\frac{d\sigma}{d\Omega}[e^+e^- \rightarrow \bar{\nu}_e \nu_e W^+ W^-] = \int_0^1 dx_1 \int_0^1 dx_2 f_{W/e}(x_1) f_{W/e}(x_2) \frac{d\hat{\sigma}}{d\hat{\Phi}} \delta(\Omega - \Omega(x_1, x_2)) \quad (35)$$

Other W, Z processes can be treated analogously.

To cut out background processes which are induced by Weizsäcker-Williams photons, it is helpful to consider the transverse momentum distribution of the W bosons. To high accuracy, the c.m. frame of γ -initiated subprocesses moves parallel to the e^\pm beams, so that these processes can be eliminated by cutting on the total transverse momentum of the subprocess with respect to the e^\pm beams. The W -initiated signal processes, by contrast, have transverse momenta of order $P_\perp(WW) \sim M_W$ so that the transverse momentum cuts have much less impact on the signal events. The luminosity spectra of the transversely/longitudinally polarized W^\pm bosons, with respect to their transverse momentum, can be written as

$$f_{W/e}^T(x, p_\perp^2) = \frac{\alpha}{4\pi s_w^2} \frac{1 + (1-x)^2}{2x} \frac{p_\perp^2}{(p_\perp^2 + (1-x)M_W^2)^2} \quad (36)$$

$$f_{W/e}^L(x, p_\perp^2) = \frac{\alpha}{4\pi s_w^2} \frac{1-x}{x} \frac{(1-x)M_W^2}{(p_\perp^2 + (1-x)M_W^2)^2} \quad (37)$$

The approximate spectra (36–37) have been derived in the limit $s \gg p_\perp^2$ and $x_{1,2}$ neither close to 0 nor 1. The accuracy of the distributions can be improved [27], however, by taking into account the exact kinematics of the vector bosons radiated from the incoming electrons/positrons. The calculation can be most conveniently performed by relating the W transverse momentum to its virtual mass squared q^2 :

$$p_\perp = \frac{\sqrt{s}}{2} (1-x) \sqrt{1 - \left[1 + \frac{2q^2}{s(1-x)}\right]^2} \quad (38)$$

with the space-like q^2 bounded by $-s(1-x) \leq q^2 \leq 0$. Expressed in terms of q^2 , the improved equivalent particle distributions can be written as

$$f_{W/e}^\lambda(x) = \frac{\alpha x}{16\pi s_w} \int_{q_{\min}^2}^{q_{\max}^2} \frac{-q^2 dq^2}{(q^2 - M_W^2)^2} \begin{cases} \frac{M_W^2 \kappa_1^2}{-q^2} & (\lambda = L) \\ (1 + \kappa_2^2) & (\lambda = T) \end{cases} \quad (39)$$

where

$$\kappa_1 \equiv \frac{2\sqrt{1-x+q^2/s}}{x-q^2/s} \quad \kappa_2 \equiv \frac{2}{x-q^2/s} - 1 \quad (40)$$

and $\lambda = L, T$ denotes longitudinal resp. transverse polarization. In the latter case we have added the results for negative and positive helicity of the W boson.

The luminosity distributions of the W bosons with respect to the transverse momentum are given as follows:

$$f_{W/e}^\lambda(x, p_\perp^2) = \frac{\alpha}{4\pi s_w^2} \begin{cases} \frac{\kappa_m x \kappa_1^2}{s \bar{x} r (\bar{x} \bar{r} + 2\kappa_m)^2} & (\lambda = L) \\ \frac{x \bar{r} (1 + \kappa_2^2)}{2sr (\bar{x} \bar{r} + 2\kappa_m)^2} & (\lambda = T) \end{cases} \quad (41)$$

with

$$\kappa_\perp \equiv \frac{p_\perp^2}{s} \quad \kappa_m \equiv \frac{M_W^2}{s} \quad r \equiv \sqrt{1 - \frac{4\kappa_\perp}{(1-x)^2}} \quad \bar{x} \equiv 1-x \quad \bar{r} \equiv 1-r \quad (42)$$

From these spectra, the transverse momentum distributions of the two-particle WW system can be derived:

$$f_{WW/ee}^{\lambda_1 \lambda_2}(x, P_\perp^2; \hat{s}) = \int_x^1 \int_0^1 dx_1 dx_2 \iint dp_{1\perp}^2 dp_{2\perp}^2 D(x) D(P_\perp^2) f_{W/e}^{\lambda_1}(x_1, p_{1\perp}^2) f_{W/e}^{\lambda_2}(x_2, p_{2\perp}^2) \quad (43)$$

with

$$D(x) = \delta(x - x_1 x_2)|_{\hat{s}=xs} \quad (44)$$

$$D(P_\perp^2) = \int_0^{2\pi} \frac{d\varphi_{12}}{2\pi} \delta(P_\perp^2 - |\vec{p}_{1\perp} + \vec{p}_{2\perp}|^2) \quad (45)$$

where φ_{12} is the azimuthal angle between the two initial W bosons in the e^+e^- c.m. frame. Due to the implicit φ_{12} -dependence in the squared transverse momentum, $|\vec{p}_{1\perp} + \vec{p}_{2\perp}|^2$, the integral in (45) is non-trivial.

The characteristic features of the luminosity spectra with respect to the transverse momentum of the WW system are exemplified in Fig.2. In Fig.2a we depict the $P_\perp(WW)$ distributions for $x_1 = x_2 = 0.5$. The probability for the emission of longitudinal W bosons is maximal around low values of $P_\perp \sim M_W/2$ and falls off rapidly with increasing transverse momentum. The spectrum of the transverse W bosons extends to much larger values of P_\perp , decreasing asymptotically like $(1/P_\perp^2) \ln(M_W^2/P_\perp^2)$. The $\gamma\gamma$ spectrum, by contrast, is strongly peaked at zero transverse momentum.

Since the phase space in (43) is restricted for a finite collider energy \sqrt{s} , the exact distributions (41) [solid lines in Fig.2a] decrease for large transverse momenta faster than the approximate distributions (36-37) [dotted].

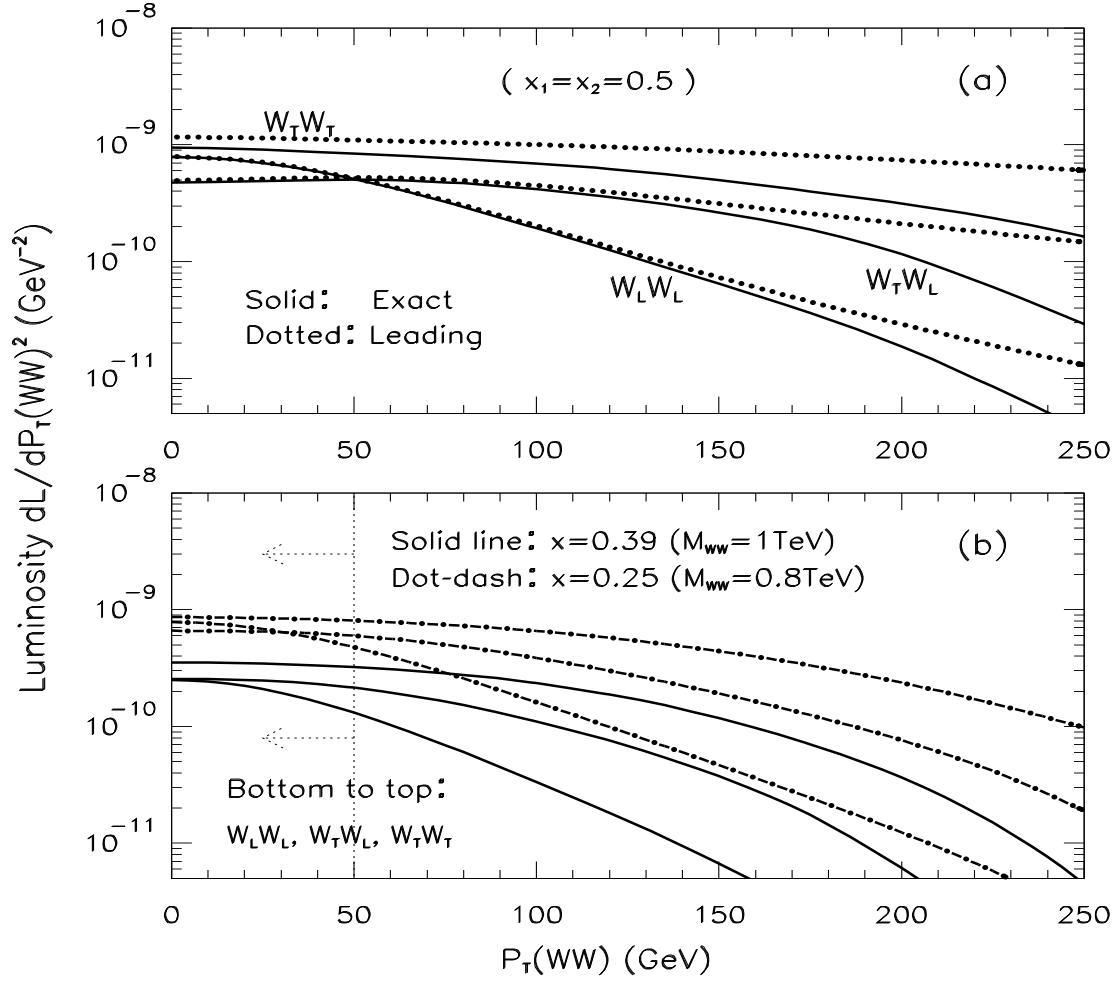


Figure 2: *Distribution of the WW transverse momentum $P_{\perp}(WW)$ in 1.6 TeV $e^{-}e^{+}/e^{-}e^{-}$ collisions.*

In Fig.2b the WW transverse momentum distributions (43) are depicted for two values of the invariant WW mass, $M_{WW} = 0.8$ and 1 TeV. A typical cut of 50 GeV is indicated by the dotted line (cf. Sec.5.). The distributions are not shown for transverse momenta beyond ~ 250 GeV since interference effects between the amplitudes become significant for large transverse momenta, invalidating the probabilistic picture of the single-particle distributions.

For higher values of M_{WW} the distributions are shifted towards lower values of P_{\perp}^2 , and the discrepancy with respect to the leading logarithmic approximation (36-37) becomes more pronounced. For this reason, the leading logarithmic approximation generally overestimates the luminosity of transverse W bosons by a factor $3 \sim 5$ [28]. We have used the improved equivalent-particle method as a guideline for the analysis and as an independent check for the complete tree-level calculation.

5. Calculation and results

For a detailed numerical study we have chosen the three processes

$$e^+e^- \rightarrow \bar{\nu}_e\nu_e W^+W^- \quad (46)$$

$$e^+e^- \rightarrow \bar{\nu}_e\nu_e ZZ \quad (47)$$

$$e^-e^- \rightarrow \nu_e\nu_e W^-W^- \quad (48)$$

where the (quasi-)elastic WW scattering signal corresponds to the generic diagrams depicted in Fig.3.

Since in all signal processes there are already two neutrinos present in the final state, important kinematic information is lost if a W boson decays leptonically (or a Z boson into two neutrinos). In particular, the c.m. energy of the subprocess cannot be determined in that case. For the present study we therefore restrict ourselves to hadronic W, Z decays and to decays of the Z boson into electrons and muons. Furthermore, an error in the dijet invariant mass is introduced by the limited energy resolution of the calorimeters, which leads to the rejection of a fraction of diboson events and to the misidentification of W *vs.* Z bosons. Adopting the results for the net efficiencies determined in Ref.[16], we assume that in a hadronic decay a true W, Z boson will be identified according to the following pattern:

$$W \rightarrow 85\% W, 10\% Z, 5\% \text{ reject} \quad (49)$$

$$Z \rightarrow 22\% W, 74\% Z, 4\% \text{ reject} \quad (50)$$

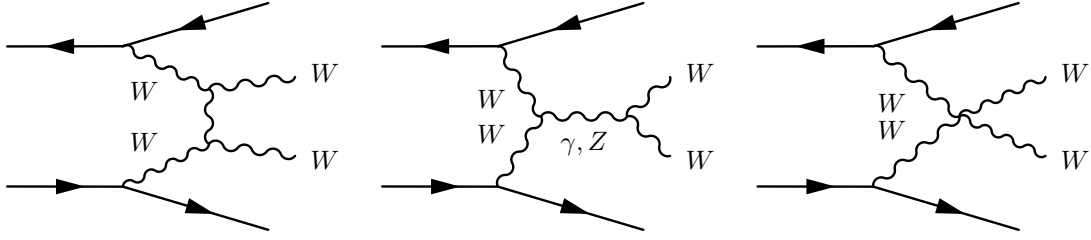


Figure 3: *Diagrams contributing to the strong WW scattering signal.*

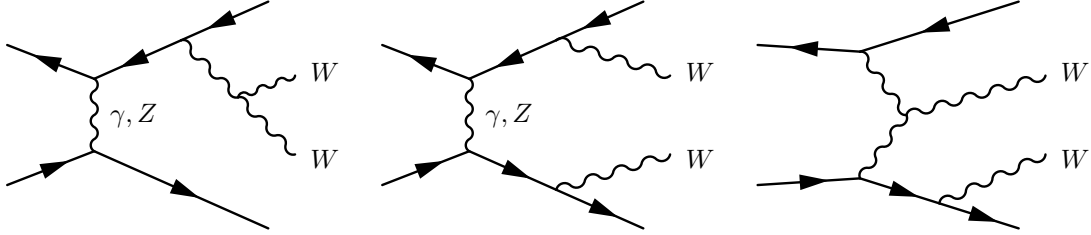


Figure 4: *Typical diagrams contributing to the irreducible background for the strong WW scattering signal.*

Using the tagging of b -quarks, the $Z \rightarrow W$ misidentification probability could be reduced, thus improving the efficiency in the ZZ channel.

However, there are also Feynman diagrams contributing to (46–48) which do not contain WW scattering as a subprocess (cf. Fig.4). This irreducible background is not negligible and must be taken into account in the analysis.

Since the final state cannot be completely resolved experimentally in all cases, further background processes will play a role (cf. Fig.5). The most important background to the signal process $e^+e^- \rightarrow \bar{\nu}\nu W^+W^-$ is generated by the reaction

$$e^+e^- \rightarrow W^+W^-e^+e^- \quad (51)$$

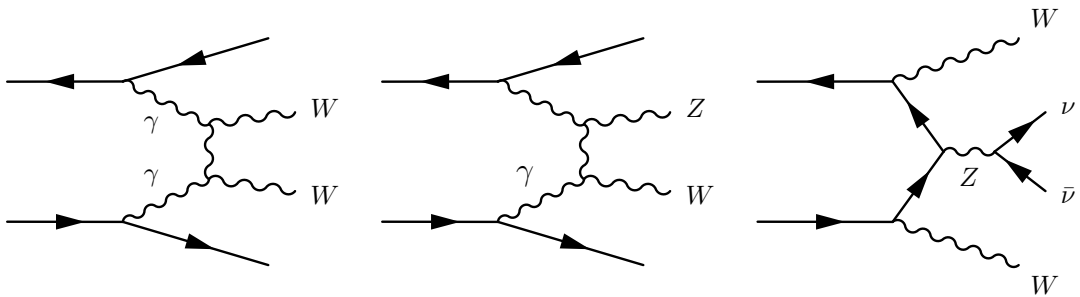


Figure 5: *Partially reducible backgrounds to the strong WW scattering signal.*

Process	800 GeV	1.6 TeV	Factor
$W^+W^-\bar{\nu}\nu$	11	56	1
$W^+W^-e^+e^-$	628	1979	1
$W^\pm Ze^\mp\nu$	39	173	0.26
$W^+W^-(Z \rightarrow \bar{\nu}\nu)$	13	11	1
$ZZ\bar{\nu}\nu$	4	26	1
ZZe^+e^-	2	4	1
$W^\pm Ze^\mp\nu$	39	173	0.12
$W^+W^-e^+e^-$	628	1979	0.01
$ZZ(Z \rightarrow \bar{\nu}\nu)$	0.6	0.4	1
$W^-W^-\nu\nu$	14	67	1

Table 2: Total cross sections in fb for various processes. Including final-state misidentification, the numbers should be multiplied by the factor given in the last column which accounts for final-state misidentification.

which is built up primarily by the subprocess $\gamma\gamma \rightarrow W^+W^-$. In this process most of the electrons/positrons are emitted in forward direction so that they cannot be detected. A similar background is introduced by the misidentification of vector bosons in jet decays:

$$e^+e^- \rightarrow W^\pm Ze^\mp\nu \quad (52)$$

An irreducible background is also generated by three-boson final states,

$$e^+e^- \rightarrow W^+W^-Z \quad (53)$$

with the Z decaying into neutrino pairs. Similar backgrounds (less dangerous for the ZZ final state) exist for the other processes.

The total cross sections for the signal and background processes, including interference effects, have been computed in a complete tree-level calculation using the automatic package CompHEP [29] in which the effective Lagrangian (6) has been implemented. The results of the cross sections for the reference point $\alpha_4 = \alpha_5 = 0$ are summarized in Tab.2.

The background reduction is essential for isolating the strong scattering signal, as demonstrated by the numbers in Tab.2. To this purpose, we follow the strategy introduced in Ref.[16]:

1. We require $M_{\text{inv}}(\bar{\nu}\nu) > 200$ (150) GeV. The first number applies for $\sqrt{s} = 1.6$ TeV, while the bracketed number for $\sqrt{s} = 800$ GeV. This cut removes the events with neutrinos

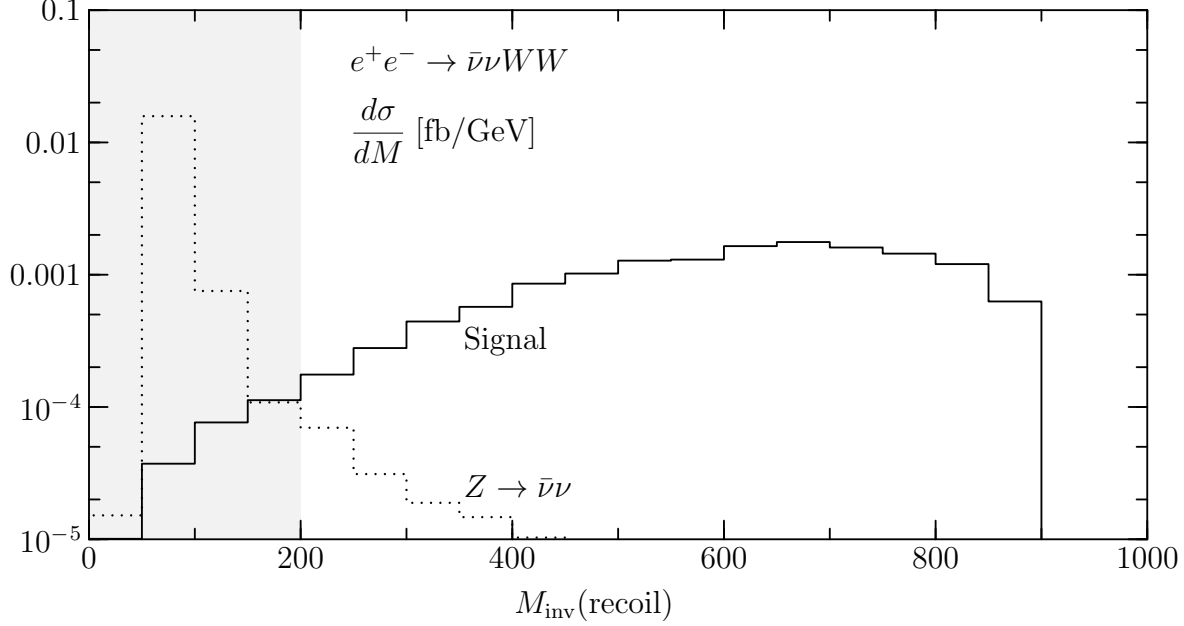


Figure 6: *Distribution of the invariant WW recoil mass distribution in the process $e^+e^- \rightarrow W^+W^-\bar{\nu}\nu$ (signal). The cut (shaded area) removes events in which the neutrinos are generated through Z decays. The other cuts are described in the text.*

from Z decay together with backgrounds from W^+W^- and QCD four-jet production. The signal is not affected (cf. Fig.6).

2. Selecting central events [$|\cos\theta(W/Z)| < 0.8$] with $p_\perp(W/Z) > 200$ (100) GeV removes events dominated by t -channel exchange in the subprocess.
3. The background from $\gamma\gamma$ fusion is reduced by two orders of magnitude if an electron veto is applied [removing events with $\theta(e) > 10^\circ$] and, at the same time, a minimum p_\perp of the vector boson pair, equivalent to the fermion p_\perp , is required. We use $p_\perp(WW) > 50$ (40) GeV and $p_\perp(ZZ) > 30$ GeV. This cut removes also about one half of the signal events. (Fig.7; cf. the discussion in Sec.4.)
4. Since the impact of the strong interaction terms \mathcal{L}_4 and \mathcal{L}_5 increases with the energy of the subprocess, we use a window in $M_{\text{inv}}(WW/ZZ)$ between 700 (350) and 1200 (600) GeV, Fig.8. [The bulk of events has lower invariant mass, but those are quite insensitive to the parameters of interest.]

After applying those cuts, we find the numbers reported in Tab.3. If they are multiplied by the misidentification probabilities in the last column, the signal/background ratios are raised

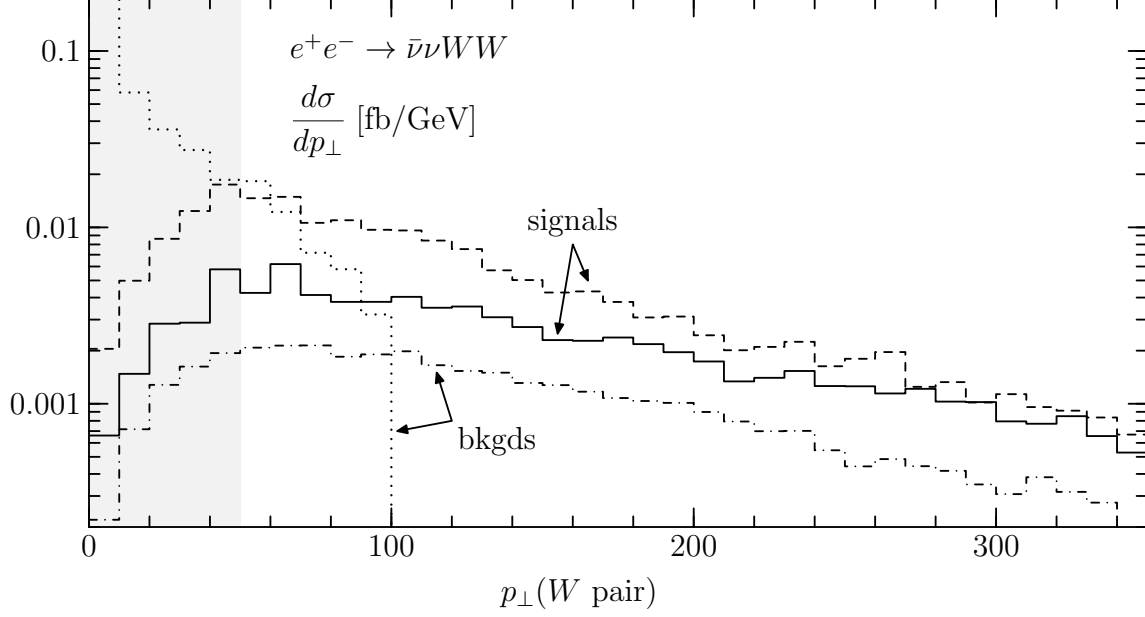


Figure 7: *Transverse momentum distribution of the W pair in the process $e^+e^- \rightarrow W^+W^-\bar{\nu}\nu$ at $\sqrt{s} = 1.6$ TeV. All cuts have been applied, but the WW reconstruction efficiency and branching ratios have not been included. The solid line corresponds to the reference point $\alpha_4 = \alpha_5 = 0$, the dashed line to $\alpha_4 = 0.005$ for comparison. The dominant backgrounds $W^+W^-e^+e^-$ (dotted) and $WZ\nu\nu$ (dot-dashed, 26% misidentification probability) are also indicated. The shaded area is removed by the p_\perp cut.*

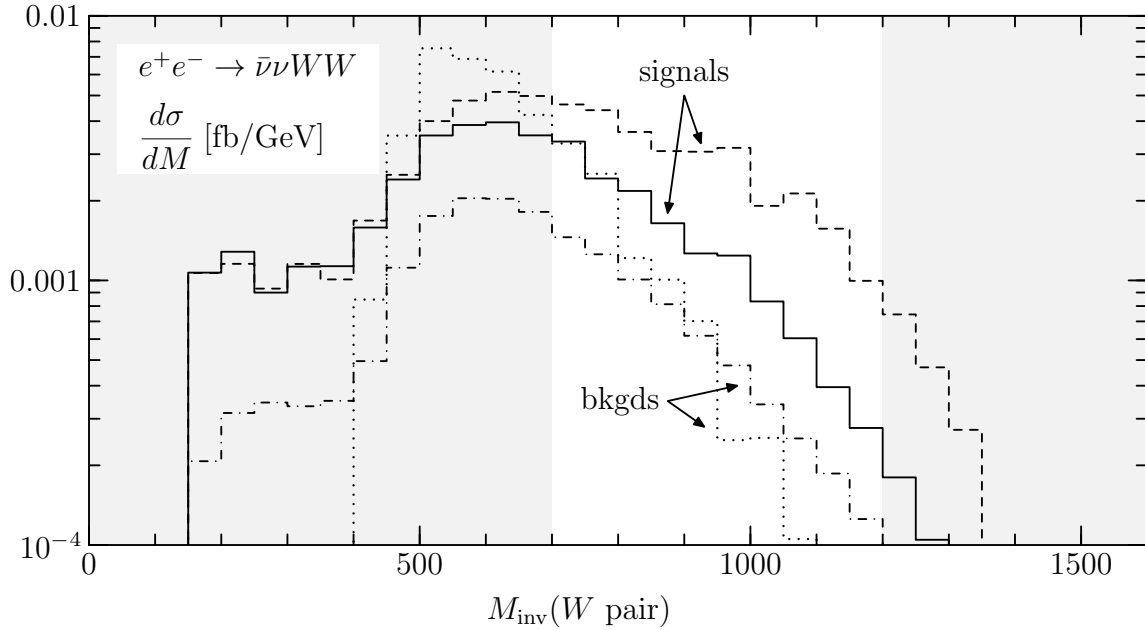


Figure 8: *Invariant mass distribution of the W pair in the process $e^+e^- \rightarrow W^+W^-\bar{\nu}\nu$. Legend as in Fig. 7.*

Process	800 GeV	1.6 TeV	Factor
$W^+W^-\bar{\nu}\nu$	0.41	0.71	1
$W^+W^-e^+e^-$	0.12	0.47	1
$W^\pm Ze^\mp\nu$	1.42	1.23	0.26
$W^+W^-(Z \rightarrow \bar{\nu}\nu)$	0.01	0.01	1
$ZZ\bar{\nu}\nu$	0.33	0.86	1
ZZe^+e^-	0.00	0.00	1
$W^\pm Ze^\mp\nu$	1.54	1.37	0.12
$W^+W^-e^+e^-$	0.51	0.93	0.01
$ZZ(Z \rightarrow \bar{\nu}\nu)$	0.00	0.00	1
$W^-W^-\nu\nu$	0.81	1.36	1

Table 3: Cross sections in fb as in Tab.2, but including all cuts.

to $\mathcal{O}(1)$. In order to obtain the final event rates, the cross sections in Tab.3 have to be multiplied by the 33% detection efficiency and the expected luminosity.

For polarized beams with left-handed electron and right-handed positron polarizations P_\mp , the rates are modified as follows:

1. Two left-handed electron/positron couplings are involved in the signal process. The rate is therefore increased by the factor $(1 + P_+)(1 + P_-)$.
2. The WZ background includes only one left-handed coupling and the cross section is therefore multiplied by the factor $1 + (P_+ + P_-)/2$.
3. The $WWee$ background is not modified. [There are diagrams in which the W 's both originate from the same fermion line. This part is modified in the same way as the WZ background; however, the increase is unimportant.]

We conclude that *both* electron and positron polarization is essential in order to improve the signal rate as well as the signal/background ratio. In the ideal case of complete polarization, S/B improves by a factor 2 and S/\sqrt{B} by a factor 3 as far as reducible backgrounds are concerned. For the irreducible part, S/\sqrt{B} increases by a factor 2 from the rate alone.

All numbers quoted so far were based on the values $\alpha_4 = \alpha_5 = 0$. Ultimately we are interested in the measurement of those parameters. The result of the theoretical prediction is depicted in Fig.9. In the upper part the dependence of the cross sections on α_4 and α_5 is

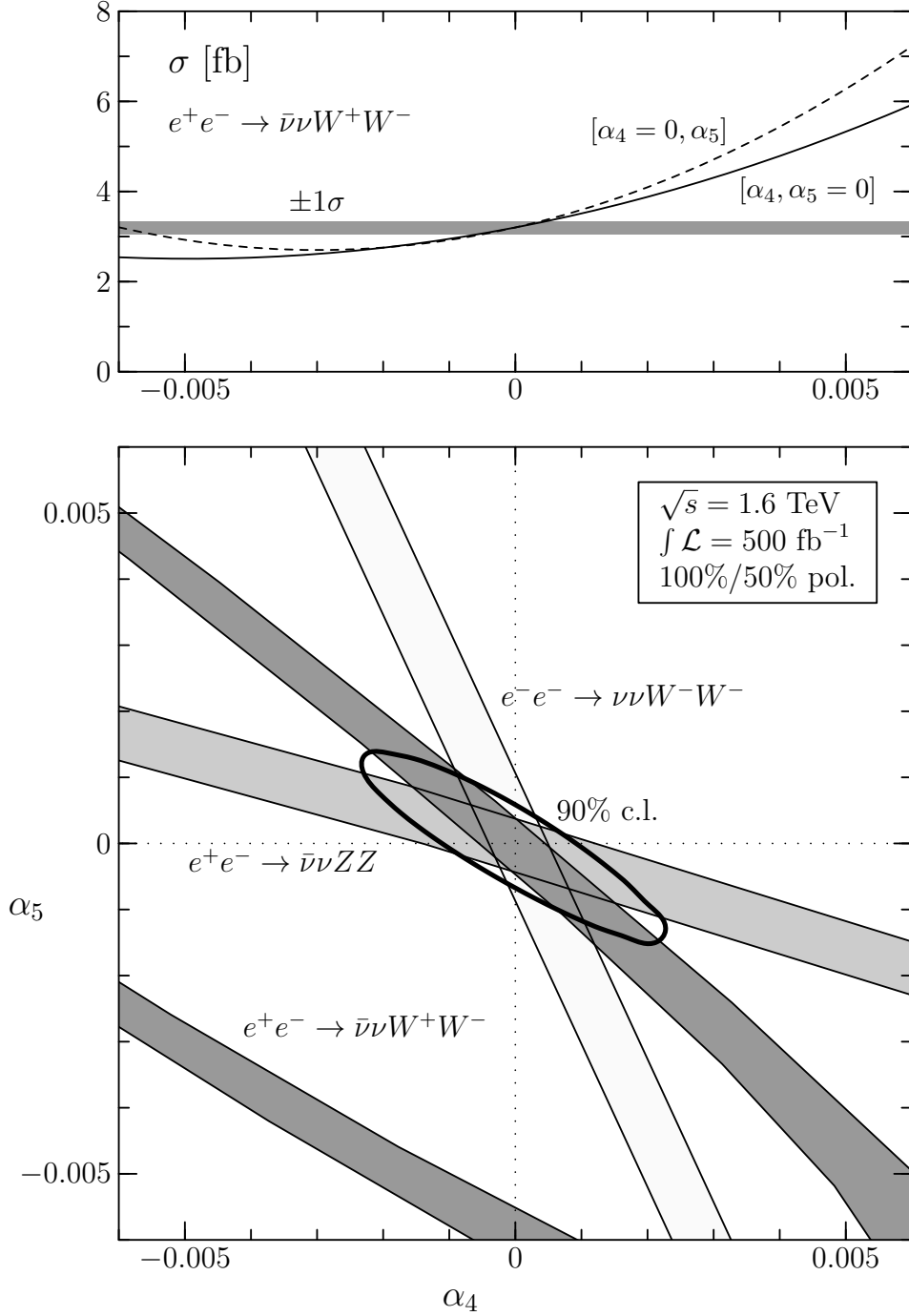


Figure 9: *Upper part:* Cross section including backgrounds for the process $e^+e^- \rightarrow \bar{\nu}\nu W^+W^-$. All cuts have been applied. The shaded band is the statistical error corresponding to the expected detection efficiency and a luminosity of $\int \mathcal{L} = 500$ fb $^{-1}$. It is assumed that the e^- (e^+) beam is polarized at a degree of 100% (50%). *Lower Part:* 1σ exclusion contours for all three processes in the α_4/α_5 plane, based on the hypothesis $\alpha_4 = \alpha_5 = 0$. The closed contour curve is the 90% exclusion limit obtained by combining the $e^+e^- \rightarrow \bar{\nu}\nu W^+W^-$ and $e^+e^- \rightarrow \bar{\nu}\nu ZZ$ channels.

displayed for polarized beams after all cuts are applied, but no detection efficiencies included. The band, based on the hypothesis $\alpha_4 = \alpha_5 = 0$, is determined by the $\pm 1\sigma$ statistical error in the $WW\bar{\nu}\nu$ event rate if the expected integrated luminosity of $\int \mathcal{L} = 500 \text{ fb}^{-1}$ and the efficiency of 33% are taken into account. The lower part of the figures shows the corresponding experimental regions in the two-dimensional $[\alpha_4, \alpha_5]$ plane, based on the hypothesis $\alpha_4 = \alpha_5 = 0$. We display the $(\pm 1\sigma)$ bounds for the individual channels, which can be combined to give the 90% exclusion limit indicated by the closed contour curve.

6. Broken custodial $SU(2)_c$

In addition to the interactions $\mathcal{L}_{4,5}$ in (15–16), three more dimension-4 operators $\mathcal{L}_{6,7,10}$ are present at next-to-leading order of the electroweak chiral Lagrangian. Since these interactions affect the quartic gauge couplings only, they also do not contribute to low-energy observables at tree level:

$$\mathcal{L}_6 = \alpha_6 \text{tr} [V_\mu V_\nu] \text{tr} [\mathcal{T}V^\mu] \text{tr} [\mathcal{T}V^\nu] \quad (54)$$

$$\mathcal{L}_7 = \alpha_7 \text{tr} [V_\mu V^\mu] \text{tr} [\mathcal{T}V_\nu] \text{tr} [\mathcal{T}V^\nu] \quad (55)$$

$$\mathcal{L}_{10} = \alpha_{10} \frac{1}{2} (\text{tr} [\mathcal{T}V^\mu] \text{tr} [\mathcal{T}V^\nu])^2 \quad (56)$$

where $\mathcal{T} = U\tau_3 U^\dagger$. Due to the presence of \mathcal{T} , the new operators $\mathcal{L}_{6,7,10}$ violate the custodial $SU(2)_c$ symmetry in contrast to $\mathcal{L}_{4,5}$.

The coefficients $\alpha_{4,5}$ and $\alpha_{6,7,10}$ can be constrained only indirectly from low-energy observables, to which they contribute through one-loop diagrams of relative magnitude $s/16\pi^2 v^2$. Since the corresponding loop divergences must be absorbed by renormalization counterterms, it is impossible to derive *precise* bounds on these parameters from low-energy data. Nevertheless, rough estimates can be obtained by keeping only the leading logarithmic terms. The estimated indirect bounds on these 4-boson couplings are summarized in the following list [30]

$$\begin{aligned} -25 \times 10^{-3} \leq \alpha_4 \leq 125 \times 10^{-3} & & -4 \times 10^{-3} \leq \alpha_6 \leq 22 \times 10^{-3} \\ -63 \times 10^{-3} \leq \alpha_5 \leq 318 \times 10^{-3} & & -32 \times 10^{-3} \leq \alpha_7 \leq 163 \times 10^{-3} \\ & & -4 \times 10^{-3} \leq \alpha_{10} \leq 22 \times 10^{-3} \end{aligned} \quad (57)$$

which are derived at 90% c.l. by setting only one new parameter nonzero at a time. Even though current bounds on the ρ parameter severely constrain the possible amount of $SU(2)_c$ violation

at leading order in the chiral expansion, the next-to-leading $SU(2)_c$ -violating parameters $\alpha_{6,7,10}$ are still allowed in the range from 0.02 to 0.2 which is well above the natural value $\sim 1/16\pi^2$.

In this section, we focus on tests of the $SU(2)_c$ -violating operators $\mathcal{L}_{6,7,10}$ in quasi-elastic WW scattering. Unlike the parameters $\alpha_{4,5}$, the terms $\alpha_{6,7,10}$ signal new dynamics beyond the standard model (SM), since the SM-like Higgs sector respects $SU(2)_c$ -symmetry and thus does not contribute to $\alpha_{6,7,10}$. The leading order of the quasi-elastic $WW \rightarrow WW$ scattering amplitudes is associated with longitudinal gauge bosons and can be written as follows:

$$A(W^+W^- \rightarrow W^+W^-) = -\frac{u}{v^2} + \frac{4(s^2 + t^2 + 2u^2)}{v^4}\alpha_4 + \frac{8(s^2 + t^2)}{v^4}\alpha_5 \quad (58)$$

$$A(W^+W^- \rightarrow ZZ) = +\frac{s}{v^2} + \frac{4(t^2 + u^2)}{v^4}(\alpha_4 + \alpha_6) + \frac{8s^2}{v^4}(\alpha_5 + \alpha_7) \quad (59)$$

$$A(W^-W^- \rightarrow W^-W^-) = -\frac{s}{v^2} + \frac{4(2s^2 + t^2 + u^2)}{v^4}\alpha_4 + \frac{8(t^2 + u^2)}{v^4}\alpha_5 \quad (60)$$

$$A(W^\pm Z \rightarrow W^\pm Z) = +\frac{t}{v^2} + \frac{4(s^2 + u^2)}{v^4}(\alpha_4 + \alpha_6) + \frac{8t^2}{v^4}(\alpha_5 + \alpha_7) \quad (61)$$

$$A(ZZ \rightarrow ZZ) = 0 + \frac{8(s^2 + t^2 + u^2)}{v^4} [(\alpha_4 + \alpha_5) + 2(\alpha_6 + \alpha_7 + \alpha_{10})] \quad (62)$$

The amplitudes are given for asymptotic energies at which the W, Z masses can be neglected.

The five parameters $\{\alpha_{4,5}; \alpha_{6,7,10}\}$ can in principle be uniquely determined by measuring the total cross sections of the processes (58–62). If the event rates are large enough, additional information can be extracted from the M_{WW} , P_\perp , and angular distributions. However, due to large backgrounds and the small eeZ coupling, the experimental analysis of the reactions (61–62) is more difficult.

Elastic $W^-W^+ \rightarrow W^-W^+$ and $W^-W^- \rightarrow W^-W^-$ scattering depends only on α_4 and α_5 ; these two processes are sufficient to determine both α_4 and α_5 to a high accuracy (Fig.9). The two reactions can therefore be taken as reference processes. The other two processes $W^-W^+ \rightarrow ZZ$ and $W^\mp Z \rightarrow W^\mp Z$ can subsequently be exploited to measure α_6 and α_7 , while α_{10} can finally be extracted from the reaction $ZZ \rightarrow ZZ$.

To probe the chiral parameters α_6 , α_7 , and α_{10} , we assume that the $SU(2)_c$ -conserving parameters α_4 and α_5 have been pre-determined in the processes $e^+e^- \rightarrow \bar{\nu}\nu W^+W^-$ and $e^-e^- \rightarrow \nu\nu W^-W^-$; in the following analysis we therefore set these parameters to the reference values $[0,0]$ *sine restructione generalitis*. In this framework, the $\pm 1\sigma$ exclusion contours for α_6

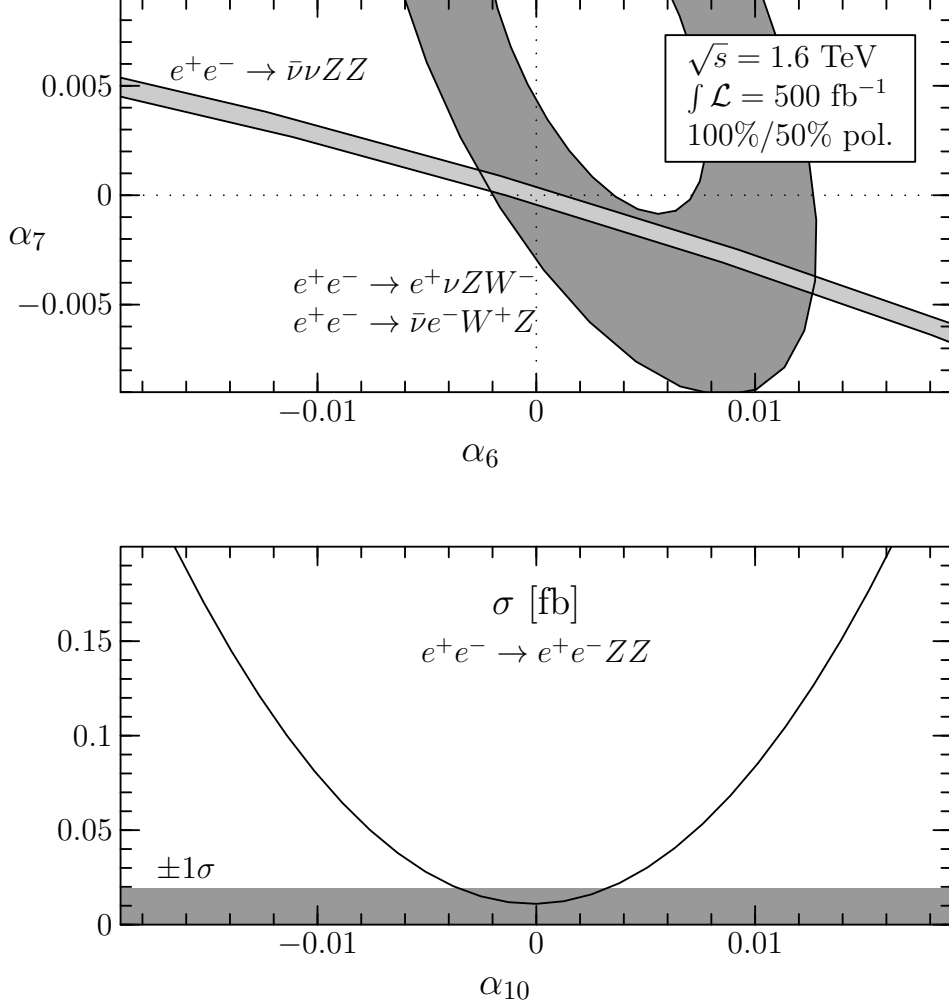


Figure 10: *Upper part*: 1σ exclusion contours for the $SU(2)_c$ -violating parameters $\alpha_{6,7}$ from $e^-e^+ \rightarrow \nu\bar{\nu}ZZ$ and $e^-e^+ \rightarrow e^-\bar{\nu}W^+Z/e^+\nu W^-Z$. *Lower part*: Cross section (including backgrounds and cuts) for $e^-e^+ \rightarrow e^-e^+ZZ$ as a probe of α_{10} . The shaded band is the statistical error corresponding to the expected detection efficiency and an integrated luminosity of 500 fb $^{-1}$.

and α_7 are shown in Fig.10a for the reactions $e^+e^- \rightarrow e^+\nu W^-Z + \text{c.c.}$ and $e^+e^- \rightarrow \nu\nu ZZ$. The $e\nu WZ$ final states suffer from large backgrounds due to γ -induced $eeWW$ events in which one e is lost in the beampipe and one W misidentified as Z . This background can be suppressed efficiently by a cut in the missing transverse momentum which in the following analysis is set to $p_\perp(\text{miss.}) > 30$ GeV.

The remaining chiral parameter α_{10} can be determined in the process $e^+e^- \rightarrow e^+e^-ZZ$. Since elastic $ZZ \rightarrow ZZ$ scattering is not possible in lowest order of the Standard Model, this channel is relatively clean, though suppressed by the small eeZ initial-state couplings. The cross section is shown as a function of α_{10} in Fig.10b. [α_{10} is actually embedded in the combination $(\alpha_4 + \alpha_5) + 2(\alpha_6 + \alpha_7) + 2\alpha_{10}$, yet the parameters $\alpha_4 \dots \alpha_7$ are assumed to be pre-determined.] From the 1σ band of the cross section we conclude that $|\alpha_{10}|$ can be bounded to less than ~ 0.005 at an e^+e^- collider of 1.6 TeV for an integrated luminosity of 500 fb^{-1} . The sensitivity is an order of magnitude better at 1.6 TeV than at 800 GeV.

7. Conclusions

As demonstrated in this analysis, $e^\pm e^-$ linear colliders operating in the TeV range are able to shed light on the details of WW scattering even in the most difficult case where no new resonances are present in the accessible energy range. The accuracy of simultaneous measurements of the chiral parameters $\alpha_{4,5}$ will be of the order 0.002 with an integrated luminosity of 500 fb^{-1} . Furthermore, the $SU(2)_c$ -violating quartic gauge couplings, $\alpha_{6,7,10}$ can be measured directly by studying all possible WW scattering channels. Analogous processes can be studied at the LHC, where a somewhat lower sensitivity on $\alpha_{4,5}$ is predicted [31]. On the other hand, if there are new resonances in WW scattering below the maximal accessible energy, they will be observed in different channels at both the LHC and $e^\pm e^-$ (or $\mu^+\mu^-$) colliders [32,16,18,33].

The error with which the reference values $[\alpha_4, \alpha_5] = [0, 0]$ of the next-to-leading corrections will be measured, can be re-interpreted as the error with which the leading amplitudes can be determined, *i.e.*, the master amplitude $A(s, t, u)_{\text{LO}} = s/F^2$. At the e^+e^- collider energy $\sqrt{s} = 1.6$ TeV, the scale parameter $F = v$ can be determined to with high accuracy

$$\Delta F/F \lesssim 5\% \tag{63}$$

for an integrated luminosity of $\int \mathcal{L} = 500 \text{ fb}^{-1}$. Since the form of this amplitude is character-

istic for the chiral symmetry breaking as the mechanism driving the dynamics of the strongly interacting W bosons, this test is the most important goal in analyzing the strong interaction threshold before resonance phenomena are expected to be observed at still higher energies. No dynamical mechanisms other than the Higgs mechanism and spontaneously broken strong interaction theories have been worked out so far through which masses of the electroweak gauge bosons could be generated in a natural way.

Acknowledgements

H.J.H is grateful to T. Han and A. Likhoded for valuable discussions. E.B. is supported by the Deutsche Forschungsgemeinschaft (DFG), H.J.H. by the Alexander von Humboldt Stiftung; W.K. by the Bundesministerium für Bildung und Forschung (BMBF); E.B. and A.P. acknowledge a grant (96-02-19773a) of the Russian Foundation of Basic Research (RFBR); C.P.Y. a NSF grant (contract PHY-9507683).

Appendix A: Unitarity bounds on α_4, α_5

If custodial $SU(2)_C$ symmetry is assumed, the weak isospin amplitudes $A^{(I)}$ ($I = 0, 1, 2$) for longitudinal WW scattering in the asymptotic regime ($|s|, |t|, |u| \gg M_W^2$) are given as follows

$$\begin{aligned} A^{(0)} &= 3A(s, t, u) + A(t, s, u) + A(u, t, s) \\ A^{(1)} &= A(t, s, u) - A(u, t, s) \\ A^{(2)} &= A(t, s, u) + A(u, t, s) \end{aligned} \quad (\text{A.64})$$

The master amplitude $A(s, t, u)$ has been discussed to next-to-leading order earlier,

$$A(s, t, u) = \frac{s}{v^2} + \alpha_4 \frac{4(t^2 + u^2)}{v^4} + \alpha_5 \frac{8s^2}{v^4} \quad (\text{A.65})$$

The isospin amplitudes may be decomposed with respect to orbital angular momentum according to

$$A^{(I)} = 32\pi \sum_{\ell=0}^{\infty} (2\ell + 1) P_{\ell}(\cos \theta) a_{\ell}^I \quad (\text{A.66})$$

From the parameterization (A.65) the non-zero amplitudes a_0^I can be extracted:

$$S \text{ wave:} \quad a_0^0 = \frac{1}{64\pi} \left[+\frac{4s}{v^2} + \frac{16}{3} (7\alpha_4 + 11\alpha_5) \frac{s^2}{v^4} \right] \quad (\text{A.67})$$

$$a_0^2 = \frac{1}{64\pi} \left[-\frac{2s}{v^2} + \frac{32}{3} (2\alpha_4 + \alpha_5) \frac{s^2}{v^4} \right] \quad (\text{A.68})$$

$$P \text{ wave:} \quad a_1^1 = \frac{1}{64\pi} \left[+\frac{2s}{3v^2} + \frac{8}{3} (\alpha_4 - 2\alpha_5) \frac{s^2}{v^4} \right] \quad (\text{A.69})$$

$$D \text{ wave:} \quad a_2^0 = \frac{1}{64\pi} \left[0 + \frac{16}{15} (2\alpha_4 + \alpha_5) \frac{s^2}{v^4} \right] \quad (\text{A.70})$$

$$a_2^2 = \frac{1}{64\pi} \left[0 + \frac{8}{15} (\alpha_4 + 2\alpha_5) \frac{s^2}{v^4} \right] \quad (\text{A.71})$$

All amplitudes with $I + \ell = \text{odd}$ vanish due to CP invariance. Angular momentum states with $\ell > 2$ are populated by higher-order operators in the chiral expansion.

Two-body elastic unitarity requires $|a_{\ell}^I - \frac{i}{2}| = 1/2$. Once a partial-wave amplitude approaches the limit $\text{Re } a_{\ell}^I = 1/2$, rescattering effects set in which induce a phase shift that unitarizes the amplitudes. Such effects can no longer be described within the effective-theory approach in a model-independent way. The validity of the chiral expansion is therefore limited to WW -scattering energies $\sqrt{\hat{s}}$ and values of the parameters α_i such that

$$|a_{\ell}^I| \lesssim 1/2 \quad . \quad (\text{A.72})$$

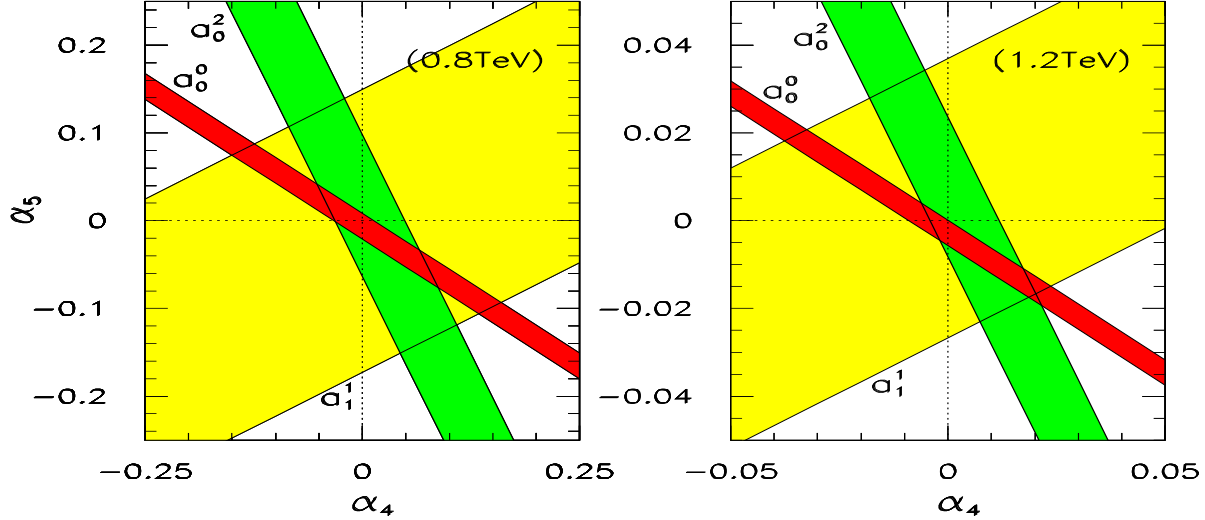


Figure 11: *Region in $\alpha_{4,5}$ allowed by tree-level unitarity for WW elastic scattering at a subprocess energy of 0.8 TeV (left) resp. 1.2 TeV (right).*

In Fig.11 we display the allowed region in the $[\alpha_4, \alpha_5]$ plane for $\sqrt{\hat{s}} = 0.8$ TeV and 1.2 TeV, which cover the main energy range of the WW scattering subprocess in the analysis. The strongest limits can be derived from unitarity in the S -wave for isospin 0 and 2 channels. The limit from the $I = \ell = 1$ channel is significantly weaker. As demonstrated in Fig.11, the unitarity bounds are very sensitive to the energy scale: For $\sqrt{\hat{s}} = 1.2$ TeV they are more stringent by about a factor of 5 than the bounds at 0.8 TeV. However, they only marginally restrict the α_i parameters in the range we are interested in ($|\alpha_i| \lesssim 0.005$). Thus they do not affect the validity of the chiral expansion in the range considered in the present analysis.

Appendix B: Radiative corrections

The leading radiative corrections of the tree-level amplitude (26) are generated by the one-loop corrections from pure Goldstone dynamics (Fig.12). They give rise to additional $SU(2)_c$ -symmetric contributions of the form [34]

$$\Delta A(s, t, u)_{1 \text{ loop}} = \frac{1}{16\pi^2 v^4} \left\{ -\frac{(t-u)}{6} \left[t \ln \frac{-t}{\mu^2} - u \ln \frac{-u}{\mu^2} \right] - \frac{s^2}{2} \ln \frac{-s}{\mu^2} \right\} \quad (\text{B.73})$$

The real part of these corrections is taken to vanish at the symmetric point $\mu^2 = s = -2t = -2u$, which corresponds to the scattering angle $\theta = \pi/2$. Infinities are absorbed in the definition

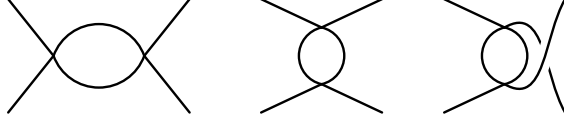


Figure 12: *Leading one-loop contributions to the WW scattering amplitude, expressed in terms of Goldstone-boson scattering.*

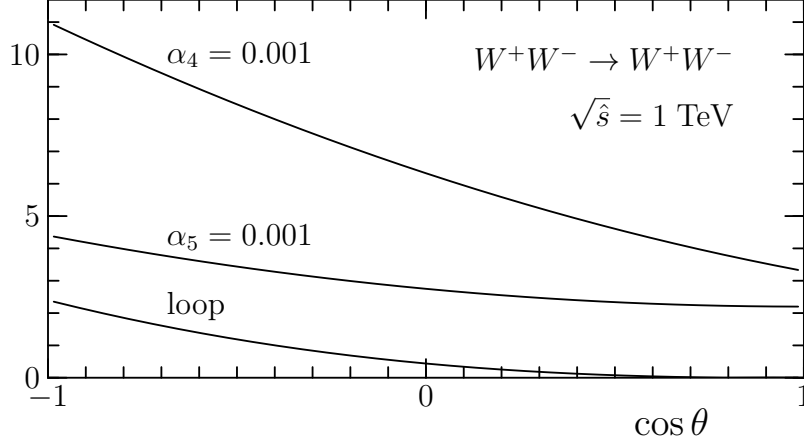


Figure 13: *Comparison of the leading one-loop corrections $|\text{Re}(\Delta A)|$ to the longitudinal $W^+W^- \rightarrow W^+W^-$ scattering amplitude, with the effects due to nonvanishing values of α_4 resp. α_5 .*

of the renormalized parameters $\alpha_{4,5}(\mu)$. A shift in the scale μ may be mapped into a finite renormalization of the parameters $\{\alpha_4, \alpha_5\}$:

$$\alpha_4(\mu) = \alpha_4(\mu_0) - \frac{1}{16\pi^2} \frac{1}{6} \ln \frac{\mu}{\mu_0} \quad (\text{B.74})$$

$$\alpha_5(\mu) = \alpha_5(\mu_0) - \frac{1}{16\pi^2} \frac{1}{12} \ln \frac{\mu}{\mu_0} \quad (\text{B.75})$$

The leading-order term $A(s, t, u)_{\text{LO}} = s/v^2$ is not renormalized. The same holds true for the next-to-leading order custodial $SU(2)_c$ -breaking coefficients $\alpha_{6,7,10}$ because standard one-loop corrections generate only $SU(2)_c$ -symmetric amplitudes.

The leading contributions are built up by Goldstone loops since contributions of transverse W, Z bosons are suppressed by the electroweak gauge couplings and by reduced enhancement factors in the energy [30].

Since the loop corrections (B.73) will affect the final results, it is necessary to estimate their impact. In Fig.13 a comparison is presented between the various contributions to the elastic scattering of longitudinal polarized W bosons, $A(W^+W^- \rightarrow W^+W^-)$, as a function of

the scattering angle. The magnitude of the loop corrections, evaluated at the renormalization point $\mu = \sqrt{\hat{s}}$, is confronted with the effects of the next-to-leading order corrections \mathcal{L}_4 and \mathcal{L}_5 on the scattering amplitude. The loop corrections are apparently significantly smaller than the chiral contributions for coefficients α_4 and $\alpha_5 = 0.001$. Since this is the size of the sensitivity we are aiming at, cf. Fig.9, we can conclude that the longitudinal loop corrections do not invalidate the previous tree-level results.

Appendix C: Decomposition of helicity amplitudes

The partial wave decomposition formula for the helicity amplitudes of the process

$$W_{\lambda_1}^a W_{\lambda_2}^b \rightarrow W_{\lambda_3}^c W_{\lambda_4}^d \quad (\text{C.76})$$

is defined as [23]

$$A(\lambda_1 \lambda_2, \lambda_3 \lambda_4) = \exp[i(\lambda - \lambda')\varphi] \sum_J A_J(\lambda_1 \lambda_2, \lambda_3 \lambda_4) d_{\lambda \lambda'}^J(\theta) \quad (\text{C.77})$$

where $\lambda \equiv \lambda_1 - \lambda_2$, $\lambda' \equiv \lambda_3 - \lambda_4$; and

$$d_{\lambda \lambda'}^J(\theta) = \sum_{s=0}^J (-)^s \frac{[(J + \lambda)!(J - \lambda)!(J + \lambda')!(J - \lambda')!]^{1/2}}{s!(J - s - \lambda)!(J - s + \lambda')!(\lambda - \lambda' + s)!} \left(\cos \frac{\theta}{2}\right)^{2(J-s)+\lambda'-\lambda} \left(-\sin \frac{\theta}{2}\right)^{2s+\lambda-\lambda'} \quad (\text{C.78})$$

Each $2 \rightarrow 2$ gauge-boson scattering process is described by a total of $3^4 = 81$ helicity amplitudes. However, by applying C,P,T transformations, they can be reduced to a basic set of 17, 20, and 13 independent amplitudes for the processes $W^+W^- \rightarrow W^+W^-$, $W^+W^- \rightarrow ZZ$, and $W^-W^- \rightarrow W^-W^-$, respectively, which we present in tabular form. In Tab.4–5 the contributions A_i to the individual helicity amplitudes which are proportional to the NLO coefficients α_i are listed. In Tab.7–8 the s -, t -channel exchange, and contact terms are presented in LO for the main process $W^+W^- \rightarrow W^+W^-$. We use the notation

$$A_J = \left(\frac{E}{M_W}\right)^{\epsilon_L} \left[\sum_V g_V^2 \left(\frac{p^2}{s - M_V^2} \hat{A}_s + \frac{E^2}{t - M_V^2} \hat{A}_t + \frac{E^2}{u - M_V^2} \hat{A}_u \right) + g^2 \hat{A}_c + g^4 \sum_{i=4,5} \alpha_i \hat{A}_i \right] \quad (\text{C.79})$$

and

$$\beta \equiv p/E \quad \beta_W \equiv p/E_W \quad \beta_Z \equiv p/E_Z \quad (\text{C.80})$$

where $p = |\vec{p}|$ is the length of 3-momentum of each incoming $W(Z)$ boson in the c.m. frame, and $E_W(E_Z)$ is the corresponding c.m. energy. When the two incoming gauge bosons have equal masses, we remove the subscript of E_W or E_Z . The vector boson masses and couplings are denoted by M_V, g_V ($V = W, Z, \gamma$ referring to the exchanged particle), where

$$g_W \equiv g = e/s_w \quad g_Z = ec_w^2/s_w \quad g_\gamma = e \quad (\text{C.81})$$

with $s_w = \sin \theta_w$, $c_w = \cos \theta_w$.

	α_4			α_5		
	$J = 0$	1	2	0	1	2
$\hat{A}_i^J(00, 00)$	$2(1 + \beta^2 + 2\beta^4)$	$2\beta^2$	2	$\frac{4}{3}(2 + 3\beta^2 + 3\beta^4)$	$-4\beta^2$	$\frac{4}{3}$
$\hat{A}_i^J(+0, 00)$	—	$-\beta^2$	$-\sqrt{3}$	—	$2\beta^2$	$-\frac{2}{\sqrt{3}}$
$\hat{A}_i^J(++ , 00)$	$-(2 + \beta^2)$	—	1	$-\frac{2}{3}(4 + 3\beta^2)$	—	$\frac{2}{3}$
$\hat{A}_i^J(+0, 0+)$	—	$-\frac{1}{2} + 2\beta^2$	3	—	2	1
$\hat{A}_i^J(+0, +0)$	—	$-\frac{1}{2} - \beta^2$	$\frac{3}{2}$	—	$1 - 2\beta^2$	1
$\hat{A}_i^J(+0, -0)$	—	$-\frac{1}{2} + \beta^2$	$-\frac{3}{2}$	—	$1 + 2\beta^2$	-1
$\hat{A}_i^J(+0, 0-)$	—	$-\frac{1}{2} - 2\beta^2$	$-\frac{3}{2}$	—	1	-1
$\hat{A}_i^J(+-, 00)$	—	—	$-\sqrt{6}$	—	—	$-\frac{2}{3}\sqrt{6}$
$\hat{A}_i^J(++ , +0)$	—	$-\frac{1}{2}$	$\frac{\sqrt{3}}{2}$	—	1	$\frac{1}{\sqrt{3}}$
$\hat{A}_i^J(++ , -0)$	—	$\frac{1}{2}$	$\frac{\sqrt{3}}{2}$	—	-1	$\frac{1}{\sqrt{3}}$
$\hat{A}_i^J(+-, +0)$	—	—	$\frac{3}{\sqrt{2}}$	—	—	$\sqrt{2}$
$\hat{A}_i^J(+-, 0+)$	—	—	$\frac{3}{\sqrt{2}}$	—	—	$\sqrt{2}$
$\hat{A}_i^J(++ , ++)$	2	$-\frac{1}{2}$	$\frac{1}{2}$	$\frac{8}{3}$	1	$\frac{1}{3}$
$\hat{A}_i^J(++ , +-)$	—	—	$-\frac{\sqrt{6}}{2}$	—	—	$-\frac{\sqrt{6}}{3}$
$\hat{A}_i^J(++ , --)$	2	$\frac{1}{2}$	$\frac{1}{2}$	$\frac{8}{3}$	-1	$\frac{1}{3}$
$\hat{A}_i^J(+-, -+)$	—	—	3	—	—	2
$\hat{A}_i^J(+-, +-)$	—	—	3	—	—	2

Table 4: *Decomposition of the NLO helicity amplitudes for $W^+W^- \rightarrow W^+W^-$.*

	$\alpha_{46} = \alpha_4 + \alpha_6$			$\alpha_{57} = \alpha_5 + \alpha_7$		
	$J = 0$	1	2	0	1	2
$\hat{A}_i^J(00, 00)$	$\frac{2}{3} + 2\beta_W^2\beta_Z^2$	—	$\frac{4}{3}$	$2(1 + \beta_W^2\beta_Z^2 + \beta_W^2 + \beta_Z^2)$	—	—
$\hat{A}_i^J(+0, 00)$	—	—	$-\frac{2}{\sqrt{3}}$	—	—	—
$\hat{A}_i^J(00, 0+)$	—	—	$-\frac{2}{\sqrt{3}}c_w^{-1}$	—	—	—
$\hat{A}_i^J(++ , 00)$	$-\frac{2}{3}$	—	$\frac{2}{3}$	$-2(1 + \beta_Z^2)$	—	—
$\hat{A}_i^J(00, ++)$	$\frac{2}{3}c_w^{-2}$	—	$\frac{2}{3}c_w^{-2}$	$-2(1 + \beta_Z^2)c_w^{-2}$	—	—
$\hat{A}_i^J(00, +-)$	—	—	$-\frac{4}{\sqrt{6}}c_w^{-2}$	—	—	—
$\hat{A}_i^J(+-, 00)$	—	—	$-\frac{4}{\sqrt{6}}$	—	—	—
$\hat{A}_i^J(+0, 0-)$	—	$-c_w^{-1}\beta_W\beta_Z$	$-c_w^{-1}$	—	—	—
$\hat{A}_i^J(+0, 0+)$	—	$c_w^{-1}\beta_W\beta_Z$	c_w^{-1}	—	—	—
$\hat{A}_i^J(++ , +0)$	—	—	$-\frac{1}{\sqrt{3}}c_w^{-1}$	—	—	—
$\hat{A}_i^J(+0, ++)$	—	—	$-\frac{1}{\sqrt{3}}c_w^{-2}$	—	—	—
$\hat{A}_i^J(++ , 0-)$	—	—	$\frac{1}{\sqrt{3}}c_w^{-1}$	—	—	—
$\hat{A}_i^J(0-, ++)$	—	—	$\frac{1}{\sqrt{3}}c_w^{-1}$	—	—	—
$\hat{A}_i^J(0+, +-)$	—	—	$\sqrt{2}c_w^{-2}$	—	—	—
$\hat{A}_i^J(+-, 0+)$	—	—	$\sqrt{2}c_w^{-1}$	—	—	—
$\hat{A}_i^J(++ , ++)$	$\frac{2}{3}c_w^{-2}$	—	$\frac{1}{3}c_w^{-2}$	$2c_w^{-2}$	—	—
$\hat{A}_i^J(++ , --)$	$\frac{2}{3}c_w^{-2}$	—	$\frac{1}{3}c_w^{-2}$	$2c_w^{-2}$	—	—
$\hat{A}_i^J(++ , +-)$	—	—	$-\frac{\sqrt{6}}{3}c_w^{-2}$	—	—	—
$\hat{A}_i^J(+-, ++)$	—	—	$-\frac{\sqrt{6}}{3}c_w^{-2}$	—	—	—
$\hat{A}_i^J(+-, -+)$	—	—	$2c_w^{-2}$	—	—	—

Table 5: *Decomposition of the NLO helicity amplitudes for $W^+W^- \rightarrow ZZ$.*

	α_4			α_5		
	$J = 0$	1	2	0	1	2
$\hat{A}_i^J(00, 00)$	$4(\frac{2}{3} + \beta^2 + \beta^4)$	—	$\frac{4}{3}$	$4(\frac{1}{3} + \beta^4)$	—	$\frac{8}{3}$
$\hat{A}_i^J(+0, 00)$	—	—	$-\frac{2}{\sqrt{3}}$	—	—	$\frac{4}{\sqrt{3}}$
$\hat{A}_i^J(++ , 00)$	$-\frac{2}{3}(4 + 3\beta^2)$	—	$-\frac{2}{3}$	$-\frac{4}{3}$	—	$\frac{4}{3}$
$\hat{A}_i^J(+0, 0+)$	—	β^2	1	—	$2\beta^2$	2
$\hat{A}_i^J(00, +-)$	—	—	$-\frac{4}{\sqrt{6}}$	—	—	$-\frac{8}{\sqrt{6}}$
$\hat{A}_i^J(+0, 0-)$	—	$-\beta^2$	-1	—	$-2\beta^2$	-2
$\hat{A}_i^J(++ , +0)$	—	—	$-\frac{1}{\sqrt{3}}$	—	—	$-\frac{2}{\sqrt{3}}$
$\hat{A}_i^J(++ , 0-)$	—	—	$\frac{1}{\sqrt{3}}$	—	—	$\frac{2}{\sqrt{3}}$
$\hat{A}_i^J(0+ , +-)$	—	—	$\sqrt{2}$	—	—	$2\sqrt{2}$
$\hat{A}_i^J(++ , ++)$	$\frac{8}{3}$	—	$\frac{1}{3}$	$\frac{3}{2}$	—	$\frac{2}{3}$
$\hat{A}_i^J(++ , +-)$	—	—	$-\frac{\sqrt{6}}{3}$	—	—	$-\frac{2\sqrt{6}}{3}$
$\hat{A}_i^J(++ , --)$	$\frac{8}{3}$	—	$\frac{1}{3}$	$\frac{4}{3}$	—	$\frac{2}{3}$
$\hat{A}_i^J(+-, -+)$	—	—	2	—	—	4

Table 6: *Decomposition of the NLO helicity amplitudes for $W^\pm W^\pm \rightarrow W^\pm W^\pm$.*

	Contact graph			s-channel Z/γ -exchange		
	$J = 0$	1	2	0	1	2
$\hat{A}_i^J(00, 00)$	$-\frac{2}{3}(1 + \beta^2)$	$6\beta^2$	$\frac{2}{3}$	—	$-4(3 - \beta^2)^2$	—
$\hat{A}_i^J(+0, 00)$	—	$-3\beta^2$	$-\frac{1}{\sqrt{3}}$	—	$8(3 - \beta^2)$	—
$\hat{A}_i^J(++ , 00)$	$\frac{2}{3} + \beta^2$	—	$\frac{1}{3}$	—	$4(\beta^2 - 3)$	—
$\hat{A}_i^J(+0, 0+)$	—	$-\frac{3}{2} + 2\beta^2$	$\frac{1}{2}$	—	-16	—
$\hat{A}_i^J(+0, +0)$	—	$-\frac{3}{2} + \beta^2$	$\frac{1}{2}$	—	-16	—
$\hat{A}_i^J(+0, -0)$	—	$-\frac{3}{2} - \beta^2$	$-\frac{1}{2}$	—	16	—
$\hat{A}_i^J(+0, 0-)$	—	$-\frac{3}{2} - 2\beta^2$	$-\frac{1}{2}$	—	16	—
$\hat{A}_i^J(+-, 00)$	—	—	$\frac{\sqrt{6}}{3}$	—	—	—
$\hat{A}_i^J(++ , +0)$	—	$\frac{3}{2}$	$-\frac{\sqrt{3}}{6}$	—	8	—
$\hat{A}_i^J(++ , -0)$	—	$\frac{3}{2}$	$\frac{\sqrt{3}}{6}$	—	-8	—
$\hat{A}_i^J(+-, +0)$	—	—	$\frac{1}{\sqrt{2}}$	—	—	—
$\hat{A}_i^J(+-, 0+)$	—	—	$\frac{1}{\sqrt{2}}$	—	—	—
$\hat{A}_i^J(++ , ++)$	$-\frac{2}{3}$	$-\frac{3}{2}$	$\frac{1}{6}$	—	-4	—
$\hat{A}_i^J(++ , +-)$	—	—	$-\frac{1}{\sqrt{6}}$	—	—	—
$\hat{A}_i^J(++ , --)$	$-\frac{2}{3}$	$\frac{3}{2}$	$\frac{1}{6}$	—	-4	—
$\hat{A}_i^J(+-, -+)$	—	—	1	—	—	—
$\hat{A}_i^J(+-, +-)$	—	—	1	—	—	—

Table 7: *Decomposition of the NLO helicity amplitudes for $W^+W^- \rightarrow W^+W^-$.*

	<i>t</i> -channel Z/γ -exchange			
	$J = 0$	1	2	3
$\hat{A}_t^J(00, 00)$	$-10(2 + \beta^2 + 4\beta^4 + \beta^6)$	$6\beta^2(-23 + 50\beta^2 - 5\beta^4)$	$20(-2 + 11\beta^2 - 10\beta^4)$	$-12\beta^2$
$\hat{A}_t^J(+0, 00)$	–	$18\beta^2(7 - 5\beta^2)$	$10\sqrt{3}(2 - 9\beta^2 + 5\beta^4)$	$4\sqrt{6}\beta^2$
$\hat{A}_t^J(++ , 00)$	$20(2 - 3\beta^2 + 2\beta^4)$	$-114\beta^2$	$20(-2 + 9\beta^2 - 2\beta^4)$	$-6\beta^2$
$\hat{A}_t^J(+0, 0+)$	–	$-6(5 + 17\beta^2 + 5\beta^4)$	$10(-3 + 13\beta^2 - 3\beta^4)$	$-8\beta^2$
$\hat{A}_t^J(+0, +0)$	–	$3(-10 - 39\beta^2 + 25\beta^4)$	$5(-6 + 25\beta^2 - 3\beta^4)$	$-8\beta^2$
$\hat{A}_t^J(+0, -0)$	–	$3(-10 + 39\beta^2 - 5\beta^4)$	$5(6 - 17\beta^2 + 3\beta^4)$	$8\beta^2$
$\hat{A}_t^J(+0, 0-)$	–	$6(-5 + 12\beta^2 - 5\beta^4)$	$10(3 - 8\beta^2 + 3\beta^4)$	$8\beta^2$
$\hat{A}_t^J(+-, 00)$	–	–	$10\sqrt{6}(2 - 5\beta^2 + 2\beta^4)$	$2\sqrt{30}\beta^2$
$\hat{A}_t^J(++ , +0)$	–	$6(5 + 13\beta^2)$	$10\sqrt{3}(1 - 5\beta^2)$	$2\sqrt{6}\beta^2$
$\hat{A}_t^J(++ , -0)$	–	$6(5 - 8\beta^2)$	$10\sqrt{3}(-1 + 2\beta^2)$	$-2\sqrt{6}\beta^2$
$\hat{A}_t^J(+-, +0)$	–	–	$10\sqrt{2}(-3 + 4\beta^2)$	$-4\sqrt{5}\beta^2$
$\hat{A}_t^J(+-, 0+)$	–	–	$10\sqrt{2}(-3 + 5\beta^2)$	$-4\sqrt{5}\beta^2$
$\hat{A}_t^J(++ , ++)$	$-5(4 + 19\beta^2)$	$-3(10 + 9\beta^2)$	$5(-2 + 13\beta^2)$	$-3\beta^2$
$\hat{A}_t^J(++ , +-)$	–	–	$5\sqrt{6}(2 - 3\beta^2)$	$\sqrt{30}\beta^2$
$\hat{A}_t^J(++ , --)$	$-5(4 + \beta^2)$	$3(10 + \beta^2)$	$5(-2 + \beta^2)$	-3β
$\hat{A}_t^J(+-, -+)$	–	–	$-10(6 + \beta^2)$	$-10\beta^2$
$\hat{A}_t^J(+-, +-)$	–	–	$-10(6 + 5\beta^2)$	$-10\beta^2$

Table 8: *Decomposition of the leading order helicity amplitudes for $W^+W^- \rightarrow W^+W^-$.*

References

- [1] B. Lee, C. Quigg and H. Thacker, Phys. Rev. Lett. **38** (1977) 883, Phys. Rev. **D16** (1977) 1519; D. Dicus and V. Mathur, Phys. Rev. **D7** (1973) 3111.
- [2] S. Glashow, Nucl. Phys. **22** (1961) 579; A. Salam, in: *Elementary Particle Theory*, ed. N. Svartholm (1968); S. Weinberg, Phys. Rev. Lett. **19** (1967) 1264.
- [3] P.W. Higgs, Phys. Lett. **12** (1964) 132, Phys. Rev. Lett. **13** (1964) 508, Phys. Rev. **145** (1966) 1156; F. Englert and R. Brout, Phys. Rev. Lett. **13** (1964) 321; G.S. Guralnik, C.R. Hagen, and T.W.B. Kibble, Phys. Rev. Lett. **13** (1964) 585; T.W.B. Kibble, Phys. Rev. **155** (1967) 1554.
- [4] C.H. Llewellyn Smith, Phys. Lett. **B46** (1973) 233; J.M. Cornwall, D.N. Levin, and G. Tiktopoulos, Phys. Rev. **D10** (1974) 1145, E: **D11** (1975) 972.
- [5] A. Blondel, in: *Proceedings of Int. Conference on High Energy Physics*, Warsaw 1996.
- [6] U. Baur and M. Demarteau, in: *Proceedings of the DPF/DPB Summer Study*, Snowmass 1996.
- [7] M.E. Peskin and T. Takeuchi, Phys. Rev. Lett. **65** (1990) 964; Phys. Rev. **D46** (1992) 381.
- [8] K.J.F. Gaemers, G.J. Gounaris, Z. Phys. **C1** (1979) 259; K. Hagiwara, K. Hikasa, R.D. Peccei, and D. Zeppenfeld, Nucl. Phys. **B282** (1987) 253; G.J. Gounaris, J.L. Kneur, D. Zeppenfeld *et al.*, *Triple Gauge Boson Couplings*, in CERN 96-01.
- [9] R. Casalbuoni, S. De Curtis, and D. Dominici, Phys. Lett. **B403** (1997) 86.
- [10] G. Bélanger and F. Boudjema, Phys. Lett. **B288** (1992) 201; S. Dawson, A. Likhoded, G. Valencia, and O. Yushchenko, in: *Proceedings of the DPF/DPB Summer Study*, Snowmass 1996, hep-ph/9610299.
- [11] S. Weinberg, Phys. Rev. **D13** (1976) 974, *ibid.* **D19** (1979) 1277; L. Susskind, Phys. Rev. **D20** (1979) 2619.
- [12] M. Veltman, Act. Phys. Pol. **B8** (1977) 475; Nucl. Phys. **B123** (1977) 89; P. Sikivie, L. Susskind, M. Voloshin, and V. Zakharov, Nucl. Phys. **B173** (1980) 189.
- [13] C.E. Vayonakis, Lett. Nuovo Cim. **17** (1976) 383; M.S. Chanowitz and M.K. Gaillard, Nucl. Phys. **B261** (1985) 379; G.J. Gounaris, R. Kögerler, and H. Neufeld, Phys. Rev. **D34** (1986) 3257; Y.-P. Yao and C.-P. Yuan, *ibid.* **D38** (1988) 2237.
- [14] H.-J. He, Y.-P. Kuang, and X.-Y. Li, Phys. Rev. Lett. **69** (1992) 2619; Phys. Lett. **B329** (1994) 278; Phys. Rev. **D49** (1994) 4842; H.-J. He, Y.-P. Kuang, and C.-P. Yuan, *ibid.* **D51** (1995) 6463; H.-J. He and W.B. Kilgore, *ibid.* **D55** (1997) 1515 and references therein.

- [15] E. Accomando *et al.* (ECFA/DESY LC Physics Working Group), DESY-97-100, hep-ph/9705442.
- [16] V. Barger, K. Cheung, T. Han, and R.J.N. Phillips, Phys. Rev. **D52** (1995) 3815.
- [17] F. Cuypers and K. Kolodziej, Phys. Lett. **B344** (1995) 365; F. Cuypers, Int. J. Mod. Phys. **A11** (1996) 1525.
- [18] T. Han, Int. J. Mod. Phys. **A11** (1996) 1541.
- [19] W. Kilian, in: *Proceedings of the DPF/DPB Summer Study*, Snowmass 1996, hep-ph/9609334; H.-J. He, DESY-97-037, in: *Proceedings of the Workshop: The Higgs Puzzle — What Can We Learn from LEP2, LHC, NLC, and FMC?*, Ringberg 1996, World Scientific.
- [20] J. Gasser and H. Leutwyler, Ann. Phys. (N.Y.) **158** (1984) 142; Nucl. Phys. **B250** (1985) 465.
- [21] T. Appelquist and C. Bernard, Phys. Rev. **D22** (1980) 200; A. Longhitano, Phys. Rev. **D22** (1980) 1166; Nucl. Phys. **B188** (1981) 118; T. Appelquist and G.-H. Wu, Phys. Rev. **D48** (1993) 3235.
- [22] S. Weinberg, Physica **96A** (1979) 327; H. Georgi, *Weak interactions and modern particle theory*, Benjamin/Cummings 1984; A. Manohar and H. Georgi, Nucl. Phys. **B234** (1984) 189.
- [23] M. Jacob and G.C. Wick, Ann. Phys. **7** (1959) 404.
- [24] M.S. Chanowitz and M.K. Gaillard, Phys. Lett. **B142** (1984) 85; G.L. Kane, W.W. Repko, and W.R. Rolnick, Phys. Lett. **B148** (1984) 367; S. Dawson, Nucl. Phys. **B249** (1985) 42; J.F. Gunion, J. Kalinowski, and A. Tofighi-Niaki, Phys. Rev. Lett. **57** (1986) 2351.
- [25] E.J. Williams, Proc. Roy. Soc. **A139** (1933) 163; Phys. Rev. **45** (1934) 729; C.F. von Weizsäcker, Z. Phys. **88** (1934) 612 .
- [26] M.S. Chen and P.M. Zerwas, Phys. Rev. **D11** (1975) 58.
- [27] P.W. Johnson, F.I. Olness, and W.-K. Tung, Phys. Rev. **D36** (1987) 291; I. Kuss and H. Spiesberger, Phys. Rev. **D53** (1996) 6078.
- [28] J.F. Gunion, J. Kalinowski, and A. Tofighi-Niaki, Phys. Rev. Lett. **57** (1986) 2351; I. Kuss and E. Nuss, Preprint BI-TP-97-16, hep-ph/9706406.
- [29] E.E. Boos, M.N. Dubinin, V.A. Ilyin, A.E. Pukhov, and V.I. Savrin, Report SNUTP-94-116, hep-ph/9503280 (unpublished); P.A. Baikov *et al.*, in: *Proceedings of the Workshop QFTHEP-96*, eds. B. Levtchenko and V. Savrin (Moscow 1996), hep-ph/9701412.

- [30] H.-J. He, Y.-P. Kuang, and C.-P. Yuan, Phys. Rev. **D55** (1997) 3038; Lectures in the Proceedings of the CCAST (World Laboratory) Workshop on *Physics at TeV Energy Scale*, Vol. 72, pp.119-234, (Beijing, 15-26 July 1996), DESY-97-056, hep-ph/9704276, and references therein.
- [31] A. Dobado, M.J. Herrero, J.R. Pelaez, E. Ruiz Morales, and M.T. Urdiales, Phys. Lett. **B352** (1995) 400; A. Dobado and M.T. Urdiales, Z. Phys. **C71** (1996) 659.
- [32] J. Bagger, V. Barger, K. Cheung, J. Gunion, T. Han, G.A. Ladinsky, R. Rosenfeld, and C.-P. Yuan, Phys. Rev. **D49** (1994) 1246; *ibid.* **D52** (1995) 3878.
- [33] V. Barger, M.S. Berger, J.F. Gunion, and T. Han, Phys. Rep. **286** (1997) 1; Phys. Rev. **D55** (1997) 142; J.F. Gunion, Preprint UCD 97-17, hep-ph/9707379.
- [34] O. Cheyette and M.K. Gaillard, Phys. Lett. **B197** (1987) 205.